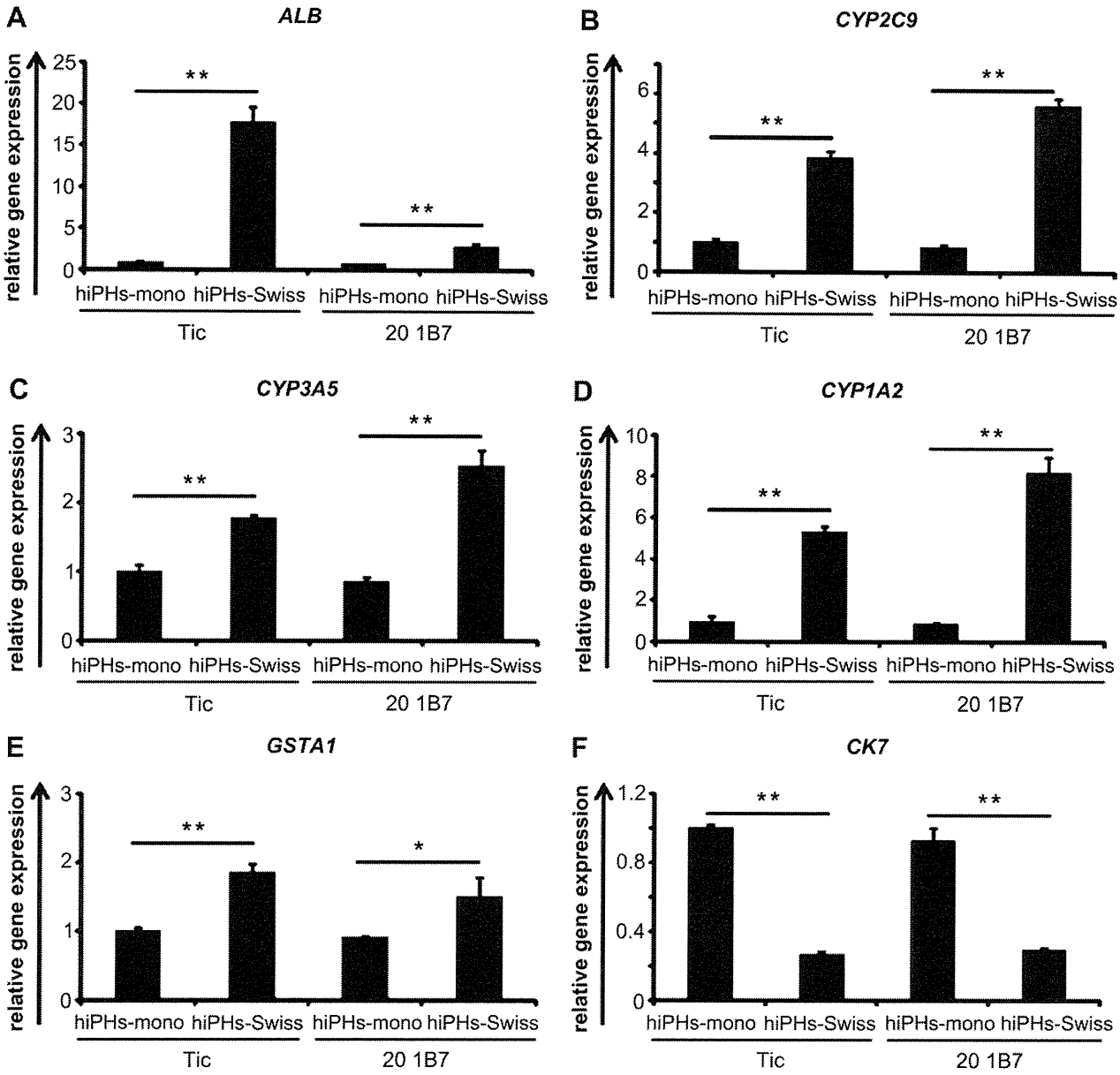

Fig. 3. Stratification of Swiss 3T3 cell sheet on hiPHs promotes hepatic maturation. Human induced pluripotent stem cells (hiPSCs) (Tic and 201B7) were differentiated into hepatocyte-like cells as described in Fig. 1A. (A–F): On day 25, the gene expression levels of *ALB* (A), *CYP2C9* (B), CYP3A5(C), *CYP1A2* (D), *GSTA1* (E), and *CK7* (F) were examined in monolayer hiPSC-derived hepatocyte-like cells (hiPHs-mono) and hiPSC-derived hepatocyte-like cells stratified with Swiss 3T3 cell sheet (hiPHs-Swiss) by real-time RT-PCR. The values were graphed as the fold-changes relative to hiPHs-mono differentiated from Tic. All data are represented as means ± SD ($n = 3$). $^{*}P < 0.05$ $^{**}P < 0.01$.

attempted to employ a cell sheet engineering technology to further induce maturation of the hEHs and hiPHs.

We observed a significant increase in the expression of hepatocyte-related genes in the hEHs- and hiPHs-Swiss as compared with those in the hEHs- and hiPHs-mono, respectively (Figs. 2 and 3), indicating that 3D co-culture with the Swiss 3T3 cell sheet was effective to promote hepatic maturation of the hEHs and hiPHs. On the other hand, Han et al. have recently shown that hESC-derived DE cells cannot be promoted to differentiate into hepatoblasts by co-culture of mouse fibroblast 3T3 cells [38]. Considering that primary rat hepatocytes are also able to grow and retain their functions for a long period of time in the presence of Swiss 3T3 cells [19,20], Swiss 3T3 cells would probably have the capacity to support the functions of freshly isolated mature hepatocytes and hESC- or hiPSC-derived hepatocyte-like cells, but not DE cells. Besides Swiss 3T3 cells, we attempted to maturate the hEHs using 3D co-culture with the bovine carotid artery endothelial cell sheet, because Kim et al. recently succeeded in creating a functional hepatocyte culture system by stacking bovine carotid artery endothelial cell sheets on primary rat hepatocytes [25]. However, our preliminary data showed that Swiss 3T3 cell sheets were superior to the bovine carotid artery endothelial cell sheets in terms of hepatic maturation of hEHs (data not shown). Thus, we conducted the present experiments to facilitate hepatic differentiation of human pluripotent stem cells using Swiss 3T3 cell sheets.

Interestingly, we found a difference in hepatic differentiation efficiency among hiPSC lines (Fig. 3). This might have been due to epigenetic memory of the hiPSC line, because several studies showed that the epigenetic memory of iPSCs affected the differentiation capacity [39,40]. Kleger et al. showed that iPSCs generated from mouse liver progenitor cells, could be more effectively differentiated into hepatocyte-like cells in comparison with iPSCs

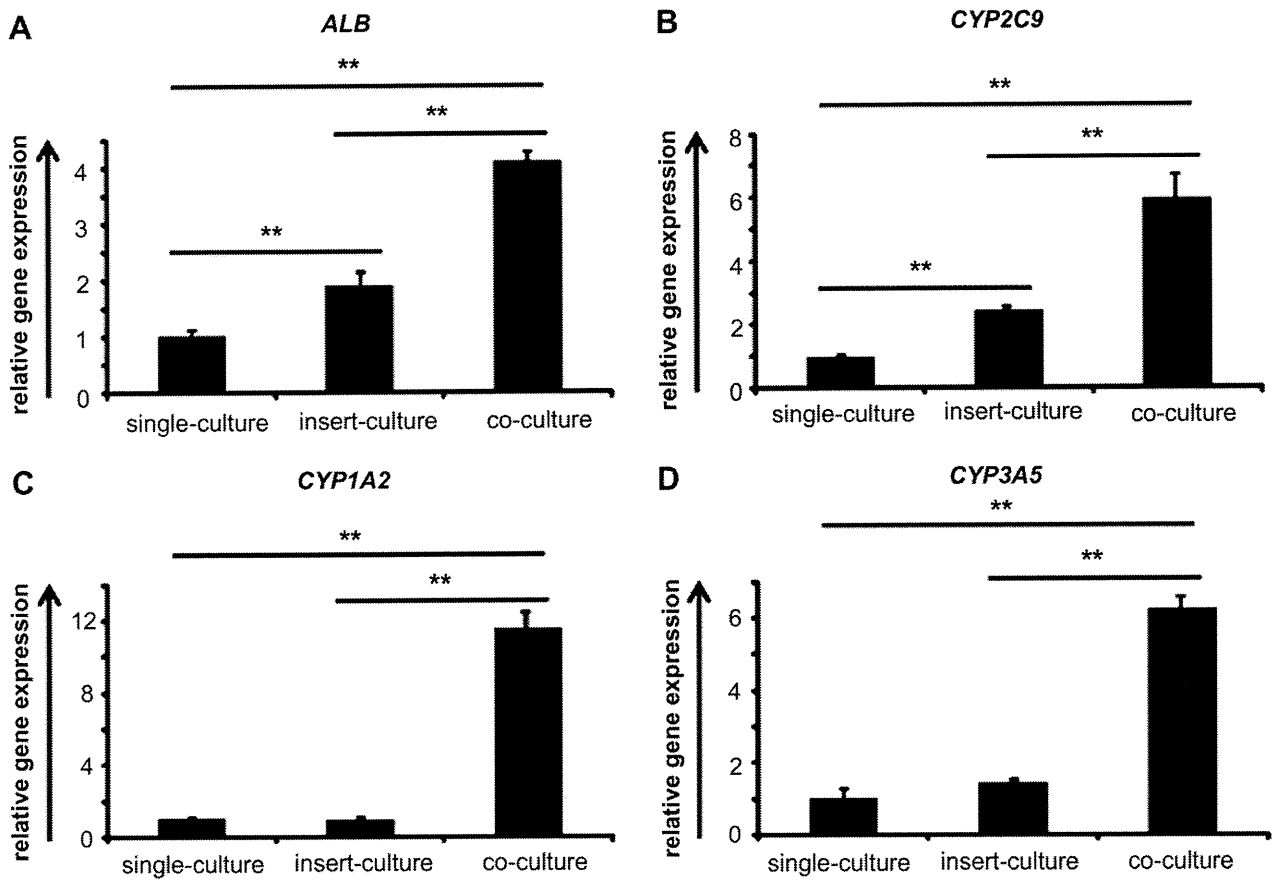

Fig. 4. Physical contacts between hESC-derived hepatocyte-like cells and Swiss 3T3 cells promote hepatic maturation. hESCs (H9) were differentiated into hepatocyte-like cells as described in Fig. 1A until day 14, and then the cells were differentiated into hepatocyte-like cells by single-culture, insert-culture, or co-culture with Swiss 3T3 cells. (A–D): On day 25, the gene expression levels of *ALB* (A), *CYP2C9* (B), *CYP1A2* (C) and *CYP3A5* (D) were examined in hESC-derived hepatocyte-like cells (hEHs) differentiated by single-culture, insert-culture, or co-culture with Swiss 3T3 cells by real-time RT-PCR. The values were graphed as the fold-changes relative to hEHs by single-culture. All data are represented as means ± SD ($n = 3$). $^{**}P < 0.01$.

generated from mouse embryo fibroblasts [41]. Thus, to more efficiently differentiate into hepatocyte-like cells from hiPSCs, it might be valuable to employ hiPSCs generated from freshly isolated human hepatocytes. Moreover, by using our 3D co-culture system, such hiPSCs would be differentiated into more mature hepatocyte-like cells.

We investigated the Swiss 3T3 cell-derived hepatic maturation factors by using cell culture inserts, and found that the physical contacts between Swiss 3T3 cells and the hEHs were the major factors contributing to the hepatic maturation of hEHs (Fig. 4). Because Swiss 3T3 cell-derived soluble factors partially induce maturation of hEHs (Fig. 4A and B), it would also be interesting to search for hepatic maturation factors secreted from Swiss 3T3 cells.

To further investigate the maturation factors, we examined whether type I collagen, which is abundantly synthesized by Swiss 3T3 cells, could promote hepatic maturation. Stratification of type I collagen gel could lead to a promotion of hepatic maturation of hEHs-mono as well as hEHs-Swiss (Fig. 5A). We also found that hepatic maturation by 3D co-culture with the Swiss 3T3 cell sheet was suppressed by inhibition of collagen synthesis (Fig. 5D). Taken together, these results show that type I collagen is one of the key molecules in promotion of hepatic maturation by stratification of Swiss 3T3 cells. It is known that the space of Disse, which faces hepatocytes directly, contains various kinds of ECM proteins, including type I collagen [42]. Because the conditions in 3D co-culture, which contains type I collagen synthesized from Swiss 3T3 cells, can mimic the *in vivo* liver microstructure, including the space of Disse, the hepatic maturation from hEHs and hiPHs might be efficiently promoted. Furthermore, it was also reported that, by the stratification of type I collagen gel in primary rat hepatocyte culture, the cytoskeletal organizations, such as actin localization, in primary rat hepatocytes were changed and stress fibers were obliterated just as in the *in vivo* state [43]. They also showed that the stratification of type I collagen gel in primary rat hepatocyte culture maintained ALB secretion in primary rat hepatocyte. Thus, the alteration of the cytoskeletal organization might also be changed in the hEHs and hiPHs by 3D co-culture with the Swiss 3T3 cell sheet. For these reasons, it could be speculated that stratification of Swiss 3T3 cell sheets positively affects the maturation process of hEHs and hiPHs mediated by cell-to-cell and cell-type I collagen–cell interactions. The expression level of the *CK7* gene in the hEHs was down-regulated by stratification of the Swiss 3T3 cell sheet or type I collagen gel (Figs. 2C and 5B). Although Matrigel, which contains large amount of type IV collagen, is widely used to differentiate hESCs and hiPSCs into hepatocyte-like cells, it is reported that type IV collagen promotes cholangiocyte differentiation [44]. Therefore, it would be important to note that stratification of Swiss 3T3 cell sheet inhibits the cholangiocyte differentiation and thereby allows the cells to drive the way to hepatic differentiation. Although we showed that a Swiss 3T3 cell-derived type I collagen plays an important role in hepatic maturation, it was likely that the other soluble factors would also be involved in the promotion of hepatic maturation.

We employed Swiss 3T3 cells for 3D co-culture with the hEHs and hiPHs. However, it would be an attractive study to employ other kinds of cells such as liver sinusoidal endothelial cells, stellate

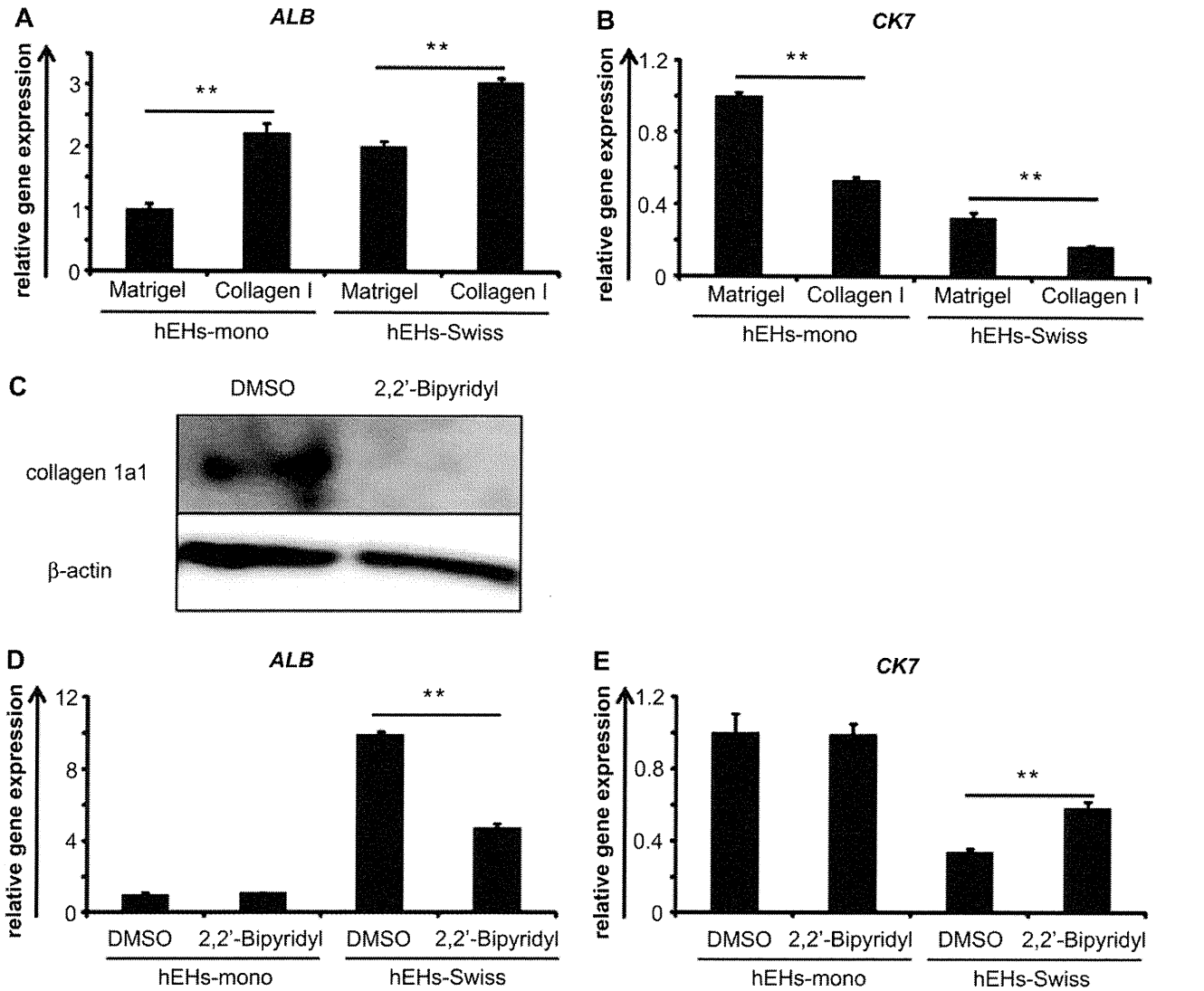

Fig. 5. Stratification of type I collagen gel promotes hepatic maturation. (A and B) hESCs (H9) were differentiated into hepatocyte-like cells as described in Fig. 1A until day 14, and then type I collagen gel (collagen I) or Matrigel are stratified on monolayer hESC-derived hepatocyte-like cells (hEHs-mono) and hESC-derived hepatocyte-like cells stratified with Swiss 3T3 cell sheet (hEHs-Swiss). On day 25, the gene expression levels of *ALB* (A) and *CK7* (B) were examined in hEHs-mono and hEHs-Swiss cultured with Matrigel or type I collagen gel by real-time RT-PCR. (C) Swiss 3T3 cells were cultured with 2,2′-Bipyridyl or solvent (0.1% DMSO) for 3 days, and then the expression of type I collagen precursor, col1a1, in these cells were detected by Western blot analysis. (D and E) hESCs (H9) were differentiated into hepatocyte-like cells as described in Fig. 1A. After stratification of Swiss 3T3 cells on day 14, these cells were treated with 2,2′-Bipyridyl or solvent (0.1% DMSO). On day 25, the gene expression levels of *ALB* (D) and *CK7* (E) were examined in hEHs-mono and hEHs-Swiss treated with 2,2′-Bipyridyl or solvent (0.1% DMSO) by real-time RT-PCR. The values were graphed as the fold-changes relative to hEHs-mono cultured with Matrigel. All data are represented as means ± SD ($n = 3$). $^{**}P < 0.01$.

cells, and Kupffer cells, to mimic the *in vivo* liver microstructure. By mimicking the *in vivo* liver microstructure, basic molecular mechanisms, including cell–cell interactions, in liver development would be clarified. Moreover, because our cell sheet technology allows us to stratify the multiple cell sheets and create layered 3D tissue constructs, combinations with multiple layers consisting of various types of cells might be able to develop an efficient method for hepatic maturation of the hEHs and hiPHs. In addition, by using new biomaterials with cell patterning techniques, more mature hepatocyte-like cells would be probably generated from human pluripotent stem cells, and thereby accelerate the research into tissue generation.

5. Conclusions

We succeeded in promoting the hepatic maturation of both the hEHs and hiPHs by stratification of the Swiss 3T3 cell sheet using a cell sheet engineering technology. We also determined that type I collagen, which is synthesized in Swiss 3T3 cells, plays an important role in hepatic maturation. Since our cell sheet engineering technology enables us to stratify multiple cell sheets, this technology would have the potential to mimic the *in vivo* liver microstructure and to generate hepatocyte-like cells, which have functions similar to primary hepatocytes. Our methods would be powerful tools for *in vitro* applications, such as drug toxicity screening in the early phase of pharmaceutical development.

Acknowledgements

We thank Misae Nishijima, Miki Yoshioka, Nobue Hirata, and Hiroko Matsumura for their excellent technical support. We also thank Tetsutaro Kikuchi (Cell Seed Inc) for providing a cell sheet stamp manipulator system. HM, KK, MKF, and TH were supported by grants from the Ministry of Health, Labor, and Welfare of Japan

(MEXT). HM was also supported by Japan Research foundation For Clinical Pharmacology and The Uehara Memorial Foundation. KO was supported by Special Coordination Funds for Promoting Science and Technology from MEXT. FS was supported by Program for Promotion of Fundamental Studies in Health Sciences of the National Institute of Biomedical Innovation (NIBIO).

Appendix A. Supplementary data

Supplementary data associated with this article can be found, in the online version, at doi:10.1016/j.biomaterials.2012.03.011.

References

[1] Thomson JA, Itskovitz-Eldor J, Shapiro SS, Waknitz MA, Swiergiel JJ, Marshall VS, et al. Embryonic stem cell lines derived from human blastocysts. Science 1998;282:1145–7.
[2] Takahashi K, Tanabe K, Ohnuki M, Narita M, Ichisaka T, Tomoda K, et al. Induction of pluripotent stem cells from adult human fibroblasts by defined factors. Cell 2007;131:861–72.
[3] Duan Y, Catana A, Meng Y, Yamamoto N, He S, Gupta S, et al. Differentiation and enrichment of hepatocyte-like cells from human embryonic stem cells in vitro and in vivo. Stem Cells 2007;25:3058–68.
[4] Touboul T, Hannan NR, Corbineau S, Martinez A, Martinet C, Branchereau S, et al. Generation of functional hepatocytes from human embryonic stem cells under chemically defined conditions that recapitulate liver development. Hepatology 2010;51:1754–65.
[5] Brolen G, Sivertsson L, Bjorquist P, Eriksson G, Ek M, Semb H, et al. Hepatocyte-like cells derived from human embryonic stem cells specifically via definitive endoderm and a progenitor stage. J Biotechnol 2010;145:284–94.
[6] Cai J, Zhao Y, Liu Y, Ye F, Song Z, Qin H, et al. Directed differentiation of human embryonic stem cells into functional hepatic cells. Hepatology 2007;45:1229–39.
[7] Snykers S, De Kock J, Rogiers V, Vanhaecke T. In vitro differentiation of embryonic and adult stem cells into hepatocytes: state of the art. Stem Cells 2009;27:577–605.
[8] Kamiya A, Kinoshita T, Miyajima A. Oncostatin M and hepatocyte growth factor induce hepatic maturation via distinct signaling pathways. FEBS Lett 2001;492:90–4.
[9] Si-Tayeb K, Lemaigre FP, Duncan SA. Organogenesis and development of the liver. Dev Cell 2010;18:175–89.
[10] Duan Y, Ma X, Zou W, Wang C, Bahbahan IS, Ahuja TP, et al. Differentiation and characterization of metabolically functioning hepatocytes from human embryonic stem cells. Stem Cells 2010;28:674–86.
[11] Inamura M, Kawabata K, Takayama K, Tashiro K, Sakurai F, Katayama K, et al. Efficient generation of hepatoblasts from human ES cells and iPS cells by transient overexpression of homeobox gene HEX. Mol Ther 2011;19:400–7.
[12] Takayama K, Inamura M, Kawabata K, Katayama K, Higuchi M, Tashiro K, et al. Efficient generation of functional hepatocytes from human embryonic stem cells and induced pluripotent stem cells by HNF4alpha transduction. Mol Ther 2012;20:127–37.
[13] Takayama K, Inamura M, Kawabata K, Tashiro K, Katayama K, Sakurai F, et al. Efficient and directive generation of two distinct endoderm lineages from human ESCs and iPSCs by differentiation stage-specific SOX17 transduction. PLoS One 2011;6:e21780.
[14] Zaret KS. Liver specification and early morphogenesis. Mech Dev 2000;92:83–8.
[15] Matsumoto K, Yoshitomi H, Rossant J, Zaret KS. Liver organogenesis promoted by endothelial cells prior to vascular function. Science 2001;294:559–63.
[16] Kinoshita T, Sekiguchi T, Xu MJ, Ito Y, Kamiya A, Tsuji K, et al. Hepatic differentiation induced by oncostatin M attenuates fetal liver hematopoiesis. Proc Natl Acad Sci USA 1999;96:7265–70.
[17] Ohashi K, Yokoyama T, Yamato M, Kuge H, Kanehiro H, Tsutsumi M, et al. Engineering functional two- and three-dimensional liver systems in vivo using hepatic tissue sheets. Nat Med 2007;13:880–5.
[18] Yamasaki C, Tateno C, Aratani A, Ohnishi C, Katayama S, Kohashi T, et al. Growth and differentiation of colony-forming human hepatocytes in vitro. J Hepatol 2006;44:749–57.
[19] Sato H, Funahashi M, Kristensen DB, Tateno C, Yoshizato K. Pleiotrophin as a Swiss 3T3 cell-derived potent mitogen for adult rat hepatocytes. Exp Cell Res 1999;246:152–64.
[20] Hui EE, Bhatia SN. Micromechanical control of cell-cell interactions. Proc Natl Acad Sci USA 2007;104:5722–6.
[21] Khetani SR, Szulgit G, Del Rio JA, Barlow C, Bhatia SN. Exploring interactions between rat hepatocytes and nonparenchymal cells using gene expression profiling. Hepatology 2004;40:545–54.
[22] Abu-Absi SF, Hansen LK, Hu WS. Three-dimensional co-culture of hepatocytes and stellate cells. Cytotechnology 2004;45:125–40.
[23] Gu J, Shi X, Zhang Y, Chu X, Hang H, Ding Y. Establishment of a three-dimensional co-culture system by porcine hepatocytes and bone marrow mesenchymal stem cells in vitro. Hepatol Res 2009;39:398–407.
[24] Thomas RJ, Bhandari R, Barrett DA, Bennett AJ, Fry JR, Powe D, et al. The effect of three-dimensional co-culture of hepatocytes and hepatic stellate cells on key hepatocyte functions in vitro. Cells Tissues Organs 2005;181:67–79.
[25] Kim K, Ohashi K, Utoh R, Kano K, Okano T. Preserved liver-specific functions of hepatocytes in 3D co-culture with endothelial cell sheets. Biomaterials 2012;33:1406–13.
[26] Harimoto M, Yamato M, Hirose M, Takahashi C, Isoi Y, Kikuchi A, et al. Novel approach for achieving double-layered cell sheets co-culture: overlaying endothelial cell sheets onto monolayer hepatocytes utilizing temperature-responsive culture dishes. J Biomed Mater Res 2002;62:464–70.
[27] Yu YD, Kim KH, Lee SG, Choi SY, Kim YC, Byun KS, et al. Hepatic differentiation from human embryonic stem cells using stromal cells. J Surg Res 2011;170:e253–61.
[28] Tuleuova N, Lee JY, Lee J, Ramanculov E, Zern MA, Revzin A. Using growth factor arrays and micropatterned co-cultures to induce hepatic differentiation of embryonic stem cells. Biomaterials 2010;31:9221–31.
[29] Miki T, Ring A, Gerlach J. Hepatic differentiation of human embryonic stem cells is promoted by three-dimensional dynamic perfusion culture conditions. Tissue Eng Part C Methods 2011;17:557–68.
[30] Kawabata K, Sakurai F, Yamaguchi T, Hayakawa T, Mizuguchi H. Efficient gene transfer into mouse embryonic stem cells with adenovirus vectors. Mol Ther 2005;12:547–54.
[31] Maizel Jr JV, White DO, Scharff MD. The polypeptides of adenovirus. I. Evidence for multiple protein components in the virion and a comparison of types 2, 7A, and 12. Virology 1968;36:115–25.
[32] Furue MK, Na J, Jackson JP, Okamoto T, Jones M, Baker D, et al. Heparin promotes the growth of human embryonic stem cells in a defined serum-free medium. Proc Natl Acad Sci USA 2008;105:13409–14.
[33] Sasagawa T, Shimizu T, Sekiya S, Haraguchi Y, Yamato M, Sawa Y, et al. Design of prevascularized three-dimensional cell-dense tissues using a cell sheet stacking manipulation technology. Biomaterials 2010;31:1646–54.
[34] Lemaigre F, Zaret KS. Liver development update: new embryo models, cell lineage control, and morphogenesis. Curr Opin Genet Dev 2004;14:582–90.
[35] Zhao R, Duncan SA. Embryonic development of the liver. Hepatology 2005;41:956–67.
[36] Suzuki A. Role for growth factors and extracellular matrix in controlling differentiation of prospectively isolated hepatic stem cells. Development 2003;130:2513–24.
[37] Goldberg B. Collagen synthesis as a marker for cell type in mouse 3T3 lines. Cell 1977;11:169–72.
[38] Han S, Dziedzic N, Gadue P, Keller GM, Gouon-Evans V. An endothelial cell niche induces hepatic specification through Dual Repression of Wnt and Notch signaling. Stem Cells 2011;29:217–28.
[39] Kim K, Doi A, Wen B, Ng K, Zhao R, Cahan P, et al. Epigenetic memory in induced pluripotent stem cells. Nature 2010;467:285–90.
[40] Polo JM, Liu S, Figueroa ME, Kulalert W, Eminli S, Tan KY, et al. Cell type of origin influences the molecular and functional properties of mouse induced pluripotent stem cells. Nat Biotechnol 2010;28:848–55.
[41] Kleger A, Mahaddalkar P, Katz SF, Lechel A, Ju JY, Loya K, et al. Increased Reprogramming capacity of mouse liver progenitor cells, compared with differentiated liver cells, Requires BAF Complex. Gastroenterology, in press.
[42] Martinez-Hernandez A. The hepatic extracellular matrix. I. Electron immunohistochemical studies in normal rat liver. Lab Invest 1984;51:57–74.
[43] Dunn JC, Tompkins RG, Yarmush ML. Long-term in vitro function of adult hepatocytes in a collagen sandwich configuration. Biotechnol Prog 1991;7:237–45.
[44] Tanimizu N, Saito H, Mostov K, Miyajima A. Long-term culture of hepatic progenitors derived from mouse Dlk+ hepatoblasts. J Cell Sci 2004;117:6425–34.

analytical chemistry

Article

pubs.acs.org/ac

Analysis of Nonhuman *N*-Glycans as the Minor Constituents in Recombinant Monoclonal Antibody Pharmaceuticals

Eiki Maeda,[†] Soichiro Kita,[‡] Mitsuhiro Kinoshita,[‡] Koji Urakami,[†] Takao Hayakawa,[§] and Kazuaki Kakehi*[,‡]

[†]Analytical Development Laboratories, CMC Center, Takeda Pharmaceutical Company Limited, Jusohonmachi 2-17-85, Yodogawa-ku, Osaka 532-8686, Japan

[‡]Faculty of Pharmaceutical Sciences, and [§]Pharmaceutical Research and Technology Institute, Kinki University, Kowakae 3-4-1, Higashi-Osaka 577-8502, Japan

Supporting Information

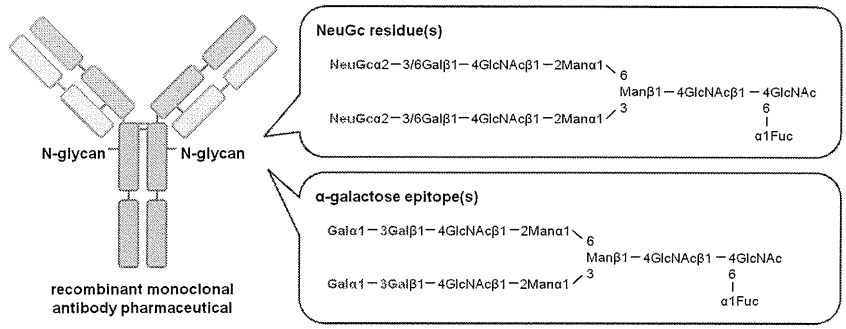

ABSTRACT: Minor N-linked glycans containing *N*-glycolylneuraminic acid residues and/or α-Gal epitopes (i.e., galactose-α1,3-galactose residues) have been reported to be present in recombinant monoclonal antibody (mAb) therapeutics. These contaminations are due to their production processes using nonhuman mammalian cell lines in culture media containing animal-derived materials. In case of the treatment of tumors, we inevitably use such mAbs by careful risk–benefit considerations to prolong patients' lives. However, expanding their clinical applications such as for rheumatism, asthma, and analgesia demands more careful evaluation of the product characteristics. The present work for detailed evaluations of *N*-glycans demonstrates the methods using capillary electrophoresis with laser-induced fluorescence detection (CE-LIF) and a combination of high-performance liquid chromatography and electrospray ionization time-of-flight mass spectrometry. The CE-LIF method provides excellent separation of both major and minor *N*-glycans from six commercial mAb pharmaceuticals within 30 min and clearly indicates that a possible trigger of immunogenicity in humans due to the presence of nonhuman *N*-glycans is present. We strongly believe that the proposed method will be a powerful tool for the analysis of *N*-glycans of recombinant mAb products in various development stages, such as clone selection, process control, and routine release testing to ensure safety and efficacy of the products.

Therapeutic recombinant monoclonal antibodies (mAbs) normally contain several N-linked glycans at asparagine residues on heavy chains.[1] The attached *N*-glycans play important biological and physicochemical roles such as resistance against protease, elongation of circulatory half-life in vivo, and antibody-dependent cellular cytotoxicity.[2−6] Although the attached *N*-glycans are mostly biantennary and core-fucosylated complex-type, their composition usually varies with the changes in manufacturing process conditions even if the same cell line is used.[7−10] In order to ensure quality of the mAb pharmaceuticals, all the *N*-glycans have to be analyzed as a critical parameter for product characterization and lot-to-lot consistency assessment.

Determination of nonhuman *N*-glycans that are not present in humans is especially important, because this will be a big problem in relation to immunogenicity and possible factor for incidence of some diseases, and possible masking of existing antigenic sites on the peptide backbone causes a crucial side effect or insufficient efficacy.[11] Recently, some important research works on the presence of nonhuman *N*-glycans in mAb products were reported. The one is galactose-α1,3-galactose (known as α-Gal epitope) attached to the non-reducing terminal of *N*-glycans. Chung et al. reported that cetuximab, a chimeric mouse–human IgG_1 mAb against the epidermal growth factor receptor produced in murine myeloma SP2/0 cell line, induced hypersensitivity reactions to subjects having IgE antibodies specific for α-Gal epitope on the Fab portion of the cetuximab heavy chain.[12] This epitope is not biosynthesized in old world monkeys, apes, humans, and CHO

Received: November 24, 2011
Accepted: February 13, 2012
Published: February 13, 2012

   dx.doi.org/10.1021/ac300234a | *Anal. Chem.* 2012, 84, 2373−2379

cells because of inactivation of the gene coding for α-1,3-galactosyltransferase (EC 2.4.1.151).[12−15] Other isotypes against the same epitope are also reported, such as IgG antibodies in serum (approximately 20−100 μg/mL) and also IgA antibodies in body secretions from saliva, milk, and colostrum.[16−18] It is now recognized that the epitope is one of the major barriers in the transplantation of organs from other mammals to humans because of inducing complement-mediated destruction and antibody-dependent cell-mediated destruction.[19,20] The other is the presence of *N*-glycolylneuraminic acid (NeuGc) residues attached to the nonreducing terminal of *N*-glycans. NeuGc cannot be synthesized in humans either, because of an irreversible mutation of the human gene *CMAH*, encoding CMP-*N*-acetylneuraminic acid hydroxylase, which is responsible for producing CMP-*N*-glycolylneuraminic acid from CMP-*N*-acetylneuraminic acid.[21,22] NeuGc exists in almost all animal cells but is not found in human tissues.[23] In several controversial reports published previously, small amounts of NeuGc have been claimed to exist in fetal human tissue, certain human tumors, and human tumor cell lines.[24,25] Normal humans have variable amounts of circulating IgA, IgM, and IgG antibodies against Neu5Gc.[26,27] Recently, Ghaderi et al. demonstrated the presence of covalently bound NeuGc in a therapeutic mAb, cetuximab, but not in panitumumab. Anti-NeuGc antibodies from healthy humans interacted with cetuximab in a NeuGc-specific manner and generated immune complexes in vitro. In addition, mice having a human-like defect in NeuGc synthesis generated antibodies to NeuGc after injection of cetuximab, and circulating anti-NeuGc antibodies can promote drug clearance.[28] These findings relevant to nonhuman *N*-glycans containing α-Gal epitopes and NeuGc residues are considered as warnings against pharmaceutical companies which have been developing therapeutic mAb pharmaceuticals.

The combination of high-performance liquid chromatography (HPLC) coupled with mass spectrometry and endoglycosidase digestion provides sufficient resolution and sensitivity for *N*-glycans.[29−34] In addition, capillary electrophoresis with laser-induced fluorescence detection (CE-LIF) has also been used for profiling of the fluorescently labeled *N*-glycans because of its throughput and high-resolution separation capability.[7,8,33−38] Chen et al. reported structural analysis of *N*-glycans of ribonuclease B, fetuin, and erythropoietin by CE-LIF after fluorescent labeling with 8-aminopyren-1,3,6-trisulfonate (APTS).[33] APTS-labeled *N*-glycans of mAbs, namely, asialo 0, 1, or 2 galactosylated biantennary complex-type *N*-glycans, were also reported.[34,36] Not only the separation methodologies described above, but also the labeling strategies of glycans for introducing a chromophore or fluorophore to the glycans with recent developments and advances of the glycan analysis, have also been published.[39−41] In the previous study, we developed an *N*-glycan profiling method for therapeutic mAb products using CE-LIF with 2-aminobenzoic acid (2-AA) as a fluorescent tag.[8] By comparison of migration times with those of 2-AA-derivatized *N*-glycans of which structures had been determined by a combination of HPLC and matrix-assisted laser desorption/ionization time-of-flight mass spectrometry (MALDI-TOF MS), all the *N*-glycans including minor species from rituximab were identified.

In the present study, we determined nonhuman *N*-glycans, the possible antigenic carbohydrate epitopes like α-Gal and NeuGc, in commercially available mAb pharmaceuticals in a detailed structural and quantitative manner using CE-LIF and a combination of HPLC and high-resolution time-of-flight mass spectrometry equipped with an electrospray ionization source and hybrid ion trap (LC/ESI-IT-TOF MS). To determine the interproduct variety of their minor *N*-glycans, chimeric Fab—human IgG_1 (cetuximab and infliximab), mouse CDR—human IgG_1 and IgG_4 (tocilizumab, bevacizumab, and gemtuzumab ozogamicin), and human IgG_1 (adalimumab) were selected and investigated. Furthermore, a lot-to-lot repetitive analysis was performed using three different lots of gemtuzumab ozogamicin in order to evaluate intraproduct variation. From the results obtained in this study, we strongly suggest that careful considerations are essentially required for assuring safety and efficacy of the therapeutic recombinant mAb products even if they are fully humanized proteins.

■ EXPERIMENTAL SECTION

Materials. Therapeutic mAb pharmaceuticals, cetuximab, infliximab, gemtuzumab ozogamicin, tocilizumab, bevacizumab, and adalimumab were donated from Kinki University Nara Hospital. γ-Globulins (human: from Cohn fraction II, III) as a human IgG antibody were purchased from Sigma (St. Louis, MO, U.S.A.). Each mAb preparation was dialyzed against distilled water for 3 days, with changing water several times at 4 °C using cellulose membrane tubing (Sanko Junyaku, Chiyoda-ku, Tokyo, Japan), and then freeze-dried. Other reagents and solvents are described in the Supporting Information.

Preparation of 2-AA-Labeled *N*-Glycans. The released *N*-glycans mixture was labeled with 2-AA according to the method reported previously.[8] After the purification of 2-AA-labeled *N*-glycans by a Sephadex LH-20 column, the collected fluorescent fraction was dried and redissolved in water (100 μL), and a portion were used for further analyses (procedures are described in the Supporting Information).

Structural Determination of the Fractionated *N*-Glycans by LC/ESI-IT-TOF MS. Structures of the *N*-glycans were analyzed by LC/ESI-IT-TOF MS (Shimadzu, Kyoto, Japan). Liquid chromatography was conducted with a CBM-20A system controller, two LC-20AD pumps, an SIL-20AC autosampler, and a CTO-20A column oven (Shimadzu). Chromatographic separation was done with a $5C_{18}$-PAQ (2.0 mm i.d. × 150 mm length, Nacalai Tesque, Kyoto, Japan) at 45 °C using a linear gradient formed by 5% acetonitrile containing 0.1% formic acid (solvent A) and 95% acetonitrile containing 0.1% formic acid (solvent B) at 0.2 mL/min. The column was initially equilibrated and eluted with 97% solvent A for 2 min, from which point solvent B was increased to 25% over 20 min and kept at this composition for additional 5 min. LC/ESI-IT-TOF MS was operated in data-dependent tandem mass spectrometry (MS/MS) mode. The curved desolvation line temperature, heat block temperature, detection voltage, and nebulizer gas flow rate were set at 200 °C, 200 °C, 1.7 kV, and 1.5 L/min, respectively. Data were collected for 80 ms for MS mode and 150 ms for MS/MS mode.

Tandem Mass Spectrometry Analysis for α-Gal-Containing *N*-Glycans by MALDI-QIT-TOF MS. For confirmation of the *N*-glycan structure containing α-Gal epitope, tandem mass analyses were conducted for several *N*-glycans by MALDI-quadrupole ion trap (QIT)-TOF mass spectrometry. MALDI-QIT-TOF mass spectra were acquired on an AXIMA-QIT-TOF mass spectrometer (Shimadzu). A nitrogen laser was used to irradiate samples, and an average shot of 50 times was taken. Argon was used for collision-

induced dissociation. The instrument was operated in positive and reflectron mode. An aqueous sample solution (2 μL) was mixed with a matrix solution (2 μL) of 1% DHB in ethanol/water (1:1), and the mixture was applied to a polished stainless-steel target and dried in atmosphere for a few hours.

CE-LIF of 2-AA-Labeled *N*-Glycans. CE-LIF was performed on a P/ACE MDQ system (Beckman Coulter, Fullerton, CA, U.S.A.) equipped with a He–Cd laser-induced fluorescence detector (ex 325 nm, em 405 nm) using a DB-1 capillary (100 μm i.d., 30 cm effective length, 40 cm total length, Agilent/J&D Scientific, Palo Alto, CA, U.S.A.) in 100 mM Tris–borate buffer (pH 8.3) containing 5% poly(ethylene glycol) as a running buffer. Poly(ethylene glycol) was added to diminish electroosmotic flow and improve the resolution. For pressure injection, sample solutions were introduced to the capillary at 1 psi for 10 s. Separation was performed at 25 kV of applied voltage at 25 °C in reverse polarity.

RESULTS AND DISCUSSION

Structural Analysis of 2-AA-Labeled *N*-Glycans by LC/ESI-IT-TOF MS and MALDI-QIT-TOF MS. The 2-AA-labeled *N*-glycans from six recombinant mAb products and a human IgG antibody were analyzed by HPLC (Figure 1), and the assigned structures of the *N*-glycans from each peak by LC/ESI-IT-TOF MS are listed on each chromatogram and summarized in Table S-1 in the Supporting Information. In total, 46 *N*-glycans were determined from the tested products. Biantennary *N*-glycans **3**, **4**, and **6** were commonly detected as major *N*-glycans in all the products, and their singly charged deprotonated molecules $[M - H]^-$ in gemtuzumab ozogamicin were observed at *m/z* 1582.6, 1744.6, and 1906.7, respectively (Table S-1 in the Supporting Information). Although agalactosylated biantennary *N*-glycan **3** was commonly observed abundantly in all products, mono- and digalactosylated biantennary *N*-glycans **4** and **6** were significantly low in bevacizumab (Figure 1c) and adalimumab (Figure 1f). In addition, the amount of digalactosylated biantennary *N*-glycan **6** in tocilizumab (Figure 1b) and cetuximab (Figure 1d) was much smaller than other mAb products, although they contained a similar amount of monogalactosylated biantennary *N*-glycan **4**. These results indicate that the variety of major *N*-glycans is remotely related to the humanization levels of mAb products.

For minor *N*-glycans (see also the enlarged chromatograms in Figure 1), tocilizumab (Figure 1b) and adalimumab (Figure 1f) contained relatively larger amounts of high-mannose-type *N*-glycans **13**–**17**, and cetuximab (Figure 1d) and infliximab (Figure 1e) contained larger amounts of hybrid-type *N*-glycans **18**–**23**, respectively. Sialylated *N*-glycans **24**–**45** were commonly observed in all mAb products. Interestingly, it was revealed that the major sialylated *N*-glycans of three mAb pharmaceuticals [gemtuzumab ozogamicin (Figure 1a), cetuximab (Figure 1d), and infliximab (Figure 1e)] were occupied with NeuGc residue **33**–**41**, **45** as identified from the results of LC/ESI-IT-TOF MS (Figure 2). Two doubly charged deprotonated molecules $[M - 2H]^{2-}$ at *m/z* 1098.3 (Figure 2a) and *m/z* 1106.3 (Figure 2b) due to *N*-glycans **26** and **36** were observed in gemtuzumab ozogamicin. Both molecules provided the same singly charged deprotonated molecule $[M - H]^-$ corresponding to digalactosylated biantennary *N*-glycan **6** in their MS/MS spectra (Figure S-1, parts a and b, in the Supporting Information). The calculated mass difference between *N*-glycans **26** and **36** was 16.0, and this clearly

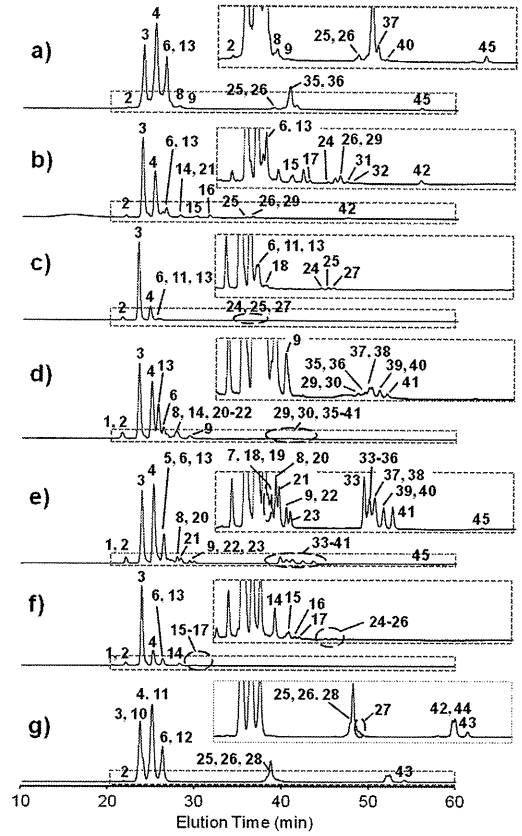

Figure 1. Analysis of 2-AA-labeled *N*-glycans by HPLC: (a) gemtuzumab ozogamicin, (b) tocilizumab, (c) bevacizumab, (d) cetuximab, (e) infliximab, (f) adalimumab, and (g) human IgG antibody. The numbers represent the *N*-glycans observed in each peak, and their structures are summarized in Table S-1 in the Supporting Information. In the box, the region between 20 and 60 min is enlarged. Analytical conditions: column, Asahi Shodex NH2P-50 4E (4.6 mm i.d. × 250 mm length); eluent, solvent A, 2% acetic acid in acetonitrile, solvent B, 5% acetic acid containing 3% triethylamine in water; gradient condition, a linear gradient (30–95% solvent B) from 2 to 82 min, keep for 15 min (95% solvent B); detection, ex 350 nm, em 425 nm.

indicated the presence of NeuGc in gemtuzumab ozogamicin. Not only gemtuzumab ozogamicin manufactured in NS0 murine myeloma cell line, but chimeric antibodies, infliximab and cetuximab, produced in murine myeloma SP2/0 cell lines, also contained NeuGc residues instead of NeuAc. The results are consistent with both the results of sialic acid analysis (see the Supporting Information) and the previous report that cetuximab has NeuGc residues at the nonreducing terminal of *N*-glycans on its Fab region.[28] In contrast, human IgG antibody and other three therapeutic mAbs manufactured in CHO cell lines, tocilizumab, bevacizumab, and adalimumab, did not contain NeuGc-containing *N*-glycans.

Two peaks (**8** and **9**) observed at 28.0 and 29.4 min in gemtuzumab ozogamicin (Figure 1a) provided doubly charged deprotonated molecules $[M - 2H]^{2-}$ at *m/z* 1033.9 (Figure 2c) and *m/z* 1115.3 (Figure 2d), respectively. The structures of these peaks were easily assigned as follows. The mass differences (Δ162.2 and Δ324.1) from digalactosylated biantennary *N*-glycan **6** indicated the presence of additional hexose molecule(s) compared to the *N*-glycan **6**. This means that one or two molecules of galactose attach to the nonreducing ends of *N*-glycan **6** to form one or two α-Gal

dx.doi.org/10.1021/ac300234a | Anal. Chem. 2012, 84, 2373–2379

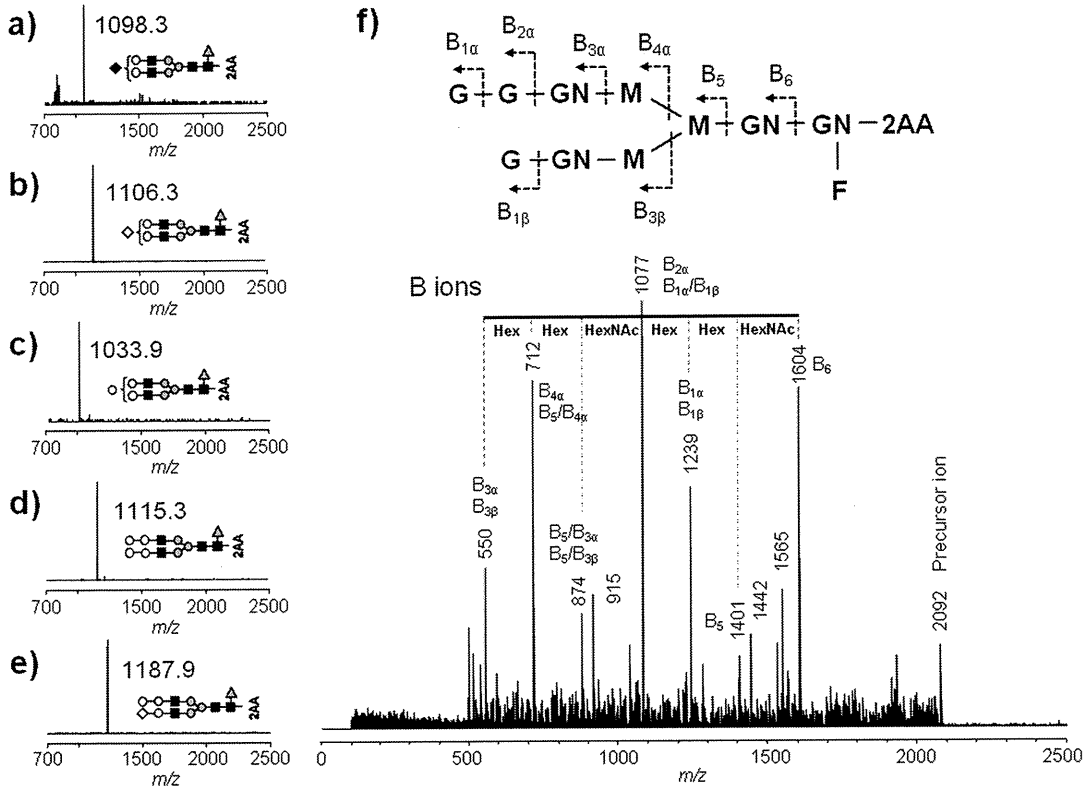

Figure 2. Negative MS spectra and positive MS/MS spectrum of 2-AA-labeled *N*-glycans from gemtuzumab ozogamicin: (a) *N*-glycan **26** containing one NeuAc residue, (b) *N*-glycan **36** containing one NeuGc residue, (c) *N*-glycan **8** containing one α-Gal epitope, (d) *N*-glycan **9** containing two α-Gal epitopes, (e) *N*-glycan **37** containing one NeuGc residue and one α-Gal epitope, and (f) *N*-glycan **8**. The dotted lines on the MS/MS spectrum indicate the type of cleavage according to Domon and Costello's nomenclature (ref 45).

epitopes. In addition, the peak detected at 41.4 min (Figure 1a) showed doubly charged deprotonated molecules $[M - 2H]^{2-}$ at *m/z* 1187.9 (Figure 2e) due to *N*-glycan **37**, and the ion provided singly charged ion $[M - H]^-$ at *m/z* 2069.8 (Figure S-1c in the Supporting Information) corresponding to *N*-glycan **8** by MS/MS analysis. These galactose residues at the nonreducing ends of *N*-glycans were specifically released by enzymatic digestion with α-galactosidase (data not shown). In addition, MS/MS analysis by MALDI-QIT-TOF MS demonstrated the presence of α-Gal epitope in its structure. Figure 2f shows the positive MS/MS spectrum of *N*-glycan **8** corresponding to the peak observed at 28.0 min in Figure 1a. The positive MS/MS spectrum derived from precursor ion $[M + Na]^+$ (*m/z* 2092.0) was mainly consisted by B-type fragment ions. The characteristic B ions at *m/z* 1401.0 (B5) and 1604.0 (B6) corresponding to a loss of 691 and 488 from $[M + Na]^+$ were observed. These mass differences corresponded to a loss of two *N*-acetylhexosamine (HexNAc) residues having a fucose residue with 2-AA and a HexNAc residue having a fucose residue with 2-AA, respectively. This result indicates that the B5 ion at 1401.0 contains three mannose and two HexNAc residues with additional three residues of hexose at the nonreducing end of *N*-glycan. The same fragment ions were observed in other mAb products as well (data not shown). These results obtained by MALDI-QIT-TOF MS obviously show the presence of α-Gal epitope in *N*-glycan **8**.

From the results described above, gemtuzumab ozogamicin contains nonhuman *N*-glycan having α-Gal epitope in its structure. Cetuximab and infliximab also contained these *N*-glycans as well (see Table S-1 in the Supporting Information), and both mAb products induced anaphylaxis mediated by IgE antibody which binds to α-Gal epitope specifically.[12,42] For infliximab, the mechanism of the anaphylaxis is under discussion, but the obtained results indicate that the presence of α-Gal epitope seems to be one of the root causes of the anaphylactic response.

The combination of HPLC and MS provides lots of structural information concerning attached *N*-glycans having NeuGc residues and α-Gal epitopes. However, due to incomplete resolution of the peaks as shown in Figure 1, detailed quantitative analysis of the *N*-glycans is a hard work. For example, two *N*-glycans, digalactosylated biantennary *N*-glycan **6** and high-mannose-type *N*-glycan **13**, which were supposed to be present in almost all mAb products, were observed at the same elution time.

CE-LIF Analysis of 2-AA-Labeled *N*-Glycans. 2-AA-labeled *N*-glycans from mAb products were analyzed by CE-LIF according to the method reported previously (Figure 3).[8] All peaks observed in each electropherogram were assigned using HPLC eluents by comparing migration times. CE-LIF provides much higher resolution than HPLC, and the *N*-glycans were observed in the order of disialo-, monosialo-, high-mannose-type, hybrid-type, and biantennary complex-type asialo-*N*-glycans. It should be noted that the *N*-glycans having the same molecular weight such as monogalactosylated biantennary complex-type *N*-glycans **4** were resolved into two peaks as indicated by asterisks in Figure 3a (at 22.3 and 22.6 min, respectively) depending on the linkage position of galactose residues at the nonreducing end. In addition, as shown in Figure 3b, digalactosylated biantennary complex-type *N*-glycan **6** and high-mannose-type *N*-glycan **13**, which could not be separated by HPLC, were completely resolved, and

dx.doi.org/10.1021/ac300234a | *Anal. Chem.* 2012, 84, 2373–2379

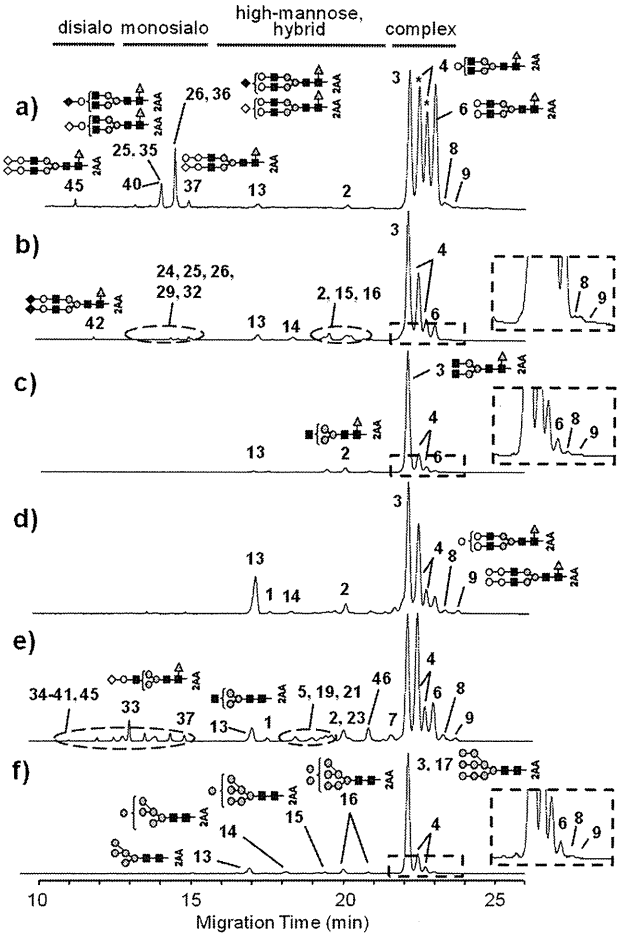

Figure 3. CE-LIF analysis of 2-AA-labeled *N*-glycans: (a) gemtuzumab ozogamicin, (b) tocilizumab, (c) bevacizumab, (d) cetuximab, (e) infliximab, and (f) adalimumab. The numbers represent the *N*-glycans observed in each peak, and their structures are summarized in Table S-1 in the Supporting Information. In the box, the region between 21.5 and 24.0 min is enlarged. Analytical conditions: capillary, DB-1 capillary (100 μm i.d., 30 cm effective length, 40 cm total length); running buffer, 100 mM Tris–borate buffer (pH 8.3) containing 5% PEG70000; injection, 1 psi for 10 s; applied voltage, −25 kV; temperature, 25 °C; detection, ex 325 nm, em 405 nm.

observed at quite different migration times. These results definitely demonstrate that CE-LIF is much more suitable for *N*-glycan profiling than HPLC because of its speed, throughput, and resolution.

From the electropherogram of gemtuzumab ozogamicin, two characteristic peaks were observed at 23.1 and 23.5 min (**8** and **9**, respectively) after four major peaks around 22 min (Figure 3a). These two peaks were observed in all the tested products but not observed in the previous study.[8] By peak assignment using fractionated HPLC eluents of gemtuzumab ozogamicin, these two peaks were identified as *N*-glycans having one and two α-Gal epitopes, respectively (Figure S-3 in the Supporting Information). In the same manner, biantennary complex-type *N*-glycans having one or two NeuGc or NeuAc residues at the nonreducing end (*N*-glycans **25**, **26**, **35**, **36**, and **45**) and hybrid-type *N*-glycan **40** containing a NeuGc residue at the nonreducing ends were also identified (Figure S-3 in the Supporting Information). However, complete separation between *N*-glycans **25** and **35** was not achieved even if using CE-LIF, because their structural difference is only the attached sialic acid types at the nonreducing end, namely, NeuGc or NeuAc. For the same reason, *N*-glycans **26** and **36** were not resolved from each other. For distinguishing terminal sialic acid species, both commonly used separation techniques in the pharmaceutical industry,[43] i.e., HPLC and CE, could not provide a complete separation because *N*-glycans usually contain six or more monosaccharides and the structural difference between NeuGc and NeuAc is much smaller (Δ16.0) than those of total masses. Terminal sialic acid modification could be alternatively accessed by sialic acid analysis, and the dominant types were over 93% as described in the Supporting Information. Therefore, we believe that current CE-LIF method is quite useful for rapid and extensive evaluation of nonhuman *N*-glycans of mAb pharmaceuticals.

The peak identification of nonhuman *N*-glycans containing NeuGc (**33**–**41** and **45**) at the nonreducing end from infliximab was also conducted by using fractionated eluents by HPLC (Figure S-4 in the Supporting Information). All the *N*-glycans having NeuGc (summarized in Table S-1 in the Supporting Information) were detected from infliximab, although one of them (*N*-glycan **39**) could not be observed by LC/ESI-IT-TOF MS. Separation between hybrid-type *N*-glycans **40** and monogalactosylated biantennary complex-type *N*-glycans **35** was achieved. The results obtained by CE-LIF indicate that the CE-LIF method affords good separation of over 40 *N*-glycans within 30 min, and the method can be used as a rapid *N*-glycan profiling in several development stages of therapeutic recombinant mAbs for monitoring and controlling product consistency as well as assuring safety and efficacy of the products.

Quantitative CE-LIF Analysis of 2-AA-Labeled *N*-Glycans. The percent compositions of detected *N*-glycans in each mAb product are summarized in Table 1. Three major *N*-glycans, **3**, **4**, and **6**, in gemtuzumab ozogamicin, tocilizumab,

Table 1. Quantitative Analysis of Attached *N*-Glycans in Recombinant mAb Products

	sialo- (%)			complex-type (%)					
product[a]	type	di-	mono-	**3**	**4**	**4**	**6**	**8, 9**	others (%)[b]
gem	NeuGc	0.4	8.9	23.9	23.1	17.5	22.1	2.3	1.8
toc	NeuAc	0.3	1.7	47.8	24.2	7.6	5.9	0.8	11.6
bev	NeuAc	0.0	0.3	75.5	12.7	3.7	1.3	1.7	6.1
cet	NeuGc	0.1	1.0	37.5	26.1	7.0	5.5	2.3	20.6
inf	NeuGc	0.1	7.4	27.6	28.7	7.9	9.0	2.4	17.1
ada	NeuAc	0.0	0.4	71.2	11.9	4.0	1.1	0.3	10.9
hIgG	NeuAc	0.6	11.1	37.8	22.7	10.9	14.0	0.0	2.9

[a]Symbols: gem, gemtuzumab ozogamicin; toc, tocilizumab; bev, bevacizumab; cet, cetuximab; inf, infliximab; ada, adalimumab; hIgG, human IgG antibody. [b]High-mannose-type and hybrid-type *N*-glycans.

dx.doi.org/10.1021/ac300234a | *Anal. Chem.* 2012, 84, 2373–2379

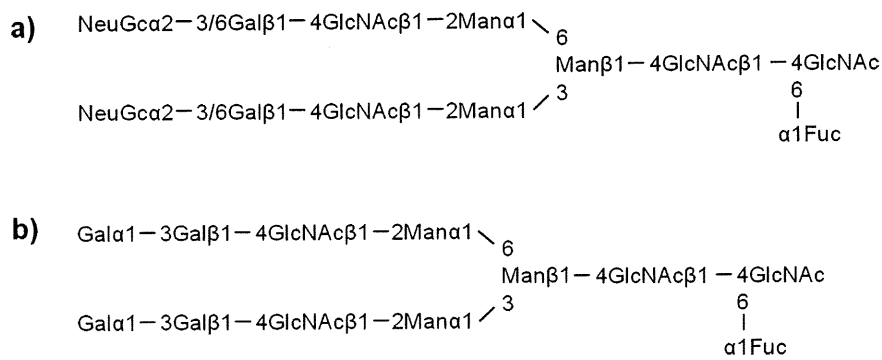

Figure 4. Representative scheme of nonhuman *N*-glycans containing NeuGc residues (a) and α-Gal epitopes (b).

bevacizumab, cetuximab, infliximab, adalimumab, and human IgG antibody (as the standard) occupied 86.6%, 85.5%, 93.2%, 76.1%, 73.2%, 88.2%, and 85.4%, respectively. For agalactosylated biantennary *N*-glycan **3**, the range of the compositions was varied from 23.9% to 75.5%. For the two peaks due to monogalactosylated biantennary complex-type *N*-glycans **4** which could be separated into two peaks, the earlier detected molecule showed a higher percent composition than the latter one in all the products. For example, these were 23.1% and 17.5% in gemtuzumab ozogamicin, respectively.

The percent compositions of minor *N*-glycans showed higher diversity than those observed for major peaks. For example, tocilizumab, cetuximab, infliximab, and adalimumab contained over 10% of high-mannose-type and hybrid-type *N*-glycans. Gemtuzumab ozogamicin and infliximab contained over 7% of monosialylated *N*-glycans of which sialic acids were exclusively NeuGc. It should be noted that all the mAb products examined in the present study except for human IgG antibody have nonhuman *N*-glycans containing α-Gal epitope(s) (**8** and **9**) as examined by CE-LIF. Again, we would like to emphasize that careful considerations are strongly needed not only for types of *N*-glycans but also for the amounts of each *N*-glycan, especially having nonhuman constituents like NeuGc residue and α-Gal epitope in their structure. It should be also emphasized that this is conveniently achieved by CE-LIF method.

Lot-to-Lot Variation of *N*-Glycan Distribution. In order to address the intraproduct variations of attached *N*-glycans, lot-to-lot analysis was performed using three different lots of gemtuzumab ozogamicin as a model mAb product. Relative standard deviations (RSDs) of percent compositions for major *N*-glycans **3**, **4**, and **6** were not higher than 2.3%, and it showed that good consistency was kept between each lot (summarized in Table S-2 in the Supporting Information). Moreover, for minor *N*-glycans having disialo-, monosialo-, and one or two α-Gal epitope(s) showed reproducible results (RSDs ≤ 5.5%). However, the sum of high-mannose-type and hybrid-type *N*-glycans showed over 10% in RSD values due to their small abundances. From the results described here, the attached *N*-glycans kept constant distributions among the production lots, although they showed wide diversity among the products due to the differences in their manufacturing process.

■ CONCLUSION

Detailed structural and quantitative analyses of N-linked glycans from six therapeutic recombinant mAb products by CE-LIF and LC/ESI-IT-TOF MS demonstrate their variety due to differences in the manufacturing process, especially cell types. Forty-six *N*-glycans were successfully assigned from the tested mAbs, and they include nonhuman *N*-glycans containing NeuGc residues instead of NeuAc (*N*-glycans **33**–**41** and **45**) and α-Gal epitope(s) (*N*-glycans **8**, **9**, and **37**). The former structure (representative structure is shown in Figure 4a) was observed in three mAb pharmaceuticals produced in nonhuman mammalian cell lines such as murine myeloma SP2/0 and NS0 cell lines, whereas it was absent in other mAbs produced in CHO cell lines. However, even if a CHO cell line is used for the production, NeuGc can be taken up and metabolically incorporated into secreted glycoprotein when animal-derived materials are used as a culture medium during the manufacturing process. Therefore, pharmaceutical companies should have their own strategy to reduce its uptake by adding a human sialic acid (i.e., NeuAc) to the culture medium.[28,44] The latter structure (Figure 4b) was observed in all the tested mAb products by CE-LIF analysis.

It should be noticed that fully humanized mAb, adalimumab, still contains α-Gal epitope. Since the detailed mechanism of this contamination is not clear, further investigation must be necessary in order to reduce or eliminate the risk of crucial side effect or insufficient efficacy in humans. Unfortunately, the detailed correlation between the risks led by these contaminations and the amount of the glycans is not still clear. Furthermore, since the peptide portion to which these nonhuman *N*-glycans are attached is not accessed in this study, it should be verified in a future work on peptide analysis of the mAb pharmaceuticals.

Hyphenated techniques of HPLC/CE with MS are powerful approaches for getting structural information, even if minor glycans are present at low levels. Actually, in tocilizumab, bevacizumab, and adalimumab, the *N*-glycans containing α-Gal epitope are present at very low levels compared to the whole amounts of *N*-glycans. When analyzed by LC/MS, as shown in Figure 1, parts b, c, and f, it was hard to detect these *N*-glycans accurately due to their very low amounts and interference by other *N*-glycans which coeluted in HPLC. In contrast, in CE-LIF, these *N*-glycans, especially *N*-glycans **8** and **9**, could be obviously separated and observed at the end of the run, around 23–24 min, as described in Figure 3, parts b, c, and f, respectively. These results clearly indicate that the CE-LIF method provides notable information regarding the presence of α-Gal epitope in mAb products rather than the HPLC method, from the aspect of glycan analysis. In the glycan analysis of mAb pharmaceuticals, both identity and quantity of nonhuman *N*-glycans are quite important information. For further investigation in order to find out the threshold of the glycan contaminations, the proposed CE-LIF method is quite useful for rapid, quantitative, and extensive evaluations of *N*-glycans of

mAb pharmaceuticals in various development stages such as, for example, clone selection, bioprocess control, detailed characterization for approval application, and lot release testing.

Although the CE/MS method for glycan analysis sounds to be a really appropriate strategy, CE cannot provide sufficient separation of *N*-glycans without the sieving effect by neutral polymers in the separation buffers. This problem leads to less quantitative information in CE/MS analysis. Therefore, when applying CE/MS to a detailed glycan analysis, this discrepancy between "resolutions of glycans" and "obtaining quantitative data" needs to be improved.

The indications of recombinant mAb products have been remarkably expanding into solid tumor, leukemia, rheumatism, asthma, and analgesia. Some of them need long-term drug exposure for obtaining sufficient results. In order to improve safety and efficacy of the products, pharmaceutical companies have to monitor and control the variations of *N*-glycans in their products especially when possible antigenic carbohydrate constituents, NeuGc residue and/or α-Gal epitope, are present, through all the development and clinical stages, even if they are fully humanized products. We believe that the present report will be a useful guide for evaluating attached *N*-glycans of mAb products.

■ ASSOCIATED CONTENT

Supporting Information

Additional information as noted in text. This material is available free of charge via the Internet at http://pubs.acs.org.

■ AUTHOR INFORMATION

Corresponding Author

*Phone: +81-6-6721-2332. Fax: +81-6-6721-2353. E-mail: k_kakehi@phar.kindai.ac.jp.

Notes

The authors declare no competing financial interest.

■ REFERENCES

(1) Sutton, B. J.; Phillips, D. C. *Biochem. Soc. Trans.* **1983**, *11*, 130–132.
(2) Tao, M. H.; Morrison, S. L. *J. Immunol.* **1989**, *143*, 2595–2601.
(3) Flintegaard, T. V.; Thygesen, P.; Rahbek-Nielsen, H.; Levery, S. B.; Kristensen, C.; Clausen, H.; Bolt, G. *Endocrinology* **2010**, *151*, 5326–5336.
(4) Umaña, P.; Jean-Mairet, J.; Moudry, R.; Amstutz, H.; Bailey, J. E. *Nat. Biotechnol.* **1999**, *17*, 176–180.
(5) Shields, R. L.; Lai, J.; Keck, R.; O'Connell, L. Y.; Hong, K.; Meng, Y. G.; Weikert, S. H. A.; Presta, L. G. *J. Biol. Chem.* **2002**, *277*, 26733–26740.
(6) Shinkawa, T.; Nakamura, K.; Yamane, N.; Shoji-Hosaka, E.; Kanda, Y.; Sakurada, M.; Uchida, K.; Anazawa, H.; Satoh, M.; Yamasaki, M.; Hanai, N.; Shitara, K. *J. Biol. Chem.* **2003**, *278*, 3466–3473.
(7) Kamoda, S.; Nomura, C.; Kinoshita, M.; Nishiura, S.; Ishikawa, R.; Kakehi, K.; Kawasaki, N.; Hayakawa, T. *J. Chromatogr., A* **2004**, *1050*, 211–216.
(8) Kamoda, S.; Ishikawa, R.; Kakehi, K. *J. Chromatogr., A* **2006**, *1133*, 332–339.
(9) Mizuochi, T.; Taniguchi, T.; Shimizu, A.; Kobata, A. *J. Immunol.* **1982**, *129*, 2016–2020.
(10) Fujii, S.; Nishiura, T.; Nishikawa, A.; Miura, R.; Taniguchi, N. *J. Biol. Chem.* **1990**, *265*, 6009–6018.
(11) Feizi, T.; Childs, R. A. *Biochem. J.* **1987**, *245*, 1–11.
(12) Chung, C. H.; Mirakhur, B.; Chan, E.; Le, Q.-T.; Berlin, J.; Morse, M.; Murphy, B. A.; Satinover, S. M.; Hosen, J.; Mauro, D.; Slebos, R. J.; Zhou, Q.; Gold, D.; Hatley, T.; Hicklin, D. J.; Platts-Mills, T. A. E. *N. Engl. J. Med.* **2008**, *358*, 1109–1117.
(13) Joziasse, D. H.; Shaper, J. H.; Jabs, E. W.; Shaper, N. L. *J. Biol. Chem.* **1991**, *266*, 6991–6998.
(14) Smith, D. F.; Larsen, R. D.; Mattox, S.; Lowe, J. B.; Cummings, R. D. *J. Biol. Chem.* **1990**, *265*, 6225–6234.
(15) Lantéri, M.; Giordanengo, V.; Vidal, F.; Gaudray, P.; Lefebvre, J.-C. *Glycobiology* **2002**, *12*, 785–792.
(16) Galili, U.; Rachmilewitz, E. A.; Peleg, A.; Flechner, I. *J. Exp. Med.* **1984**, *160*, 1519–1531.
(17) Galili, U. *Springer Semin. Immunopathol.* **1993**, *15*, 155–171.
(18) Galili, U. *Transplantation* **2004**, *78*, 1093–1098.
(19) Macher, B. A.; Galili, U. *Biochim. Biophys. Acta* **2008**, *1780*, 75–88.
(20) Kobayashi, T.; Cooper, D. K. *Subcell. Biochem.* **1999**, *32*, 229–257.
(21) Varki, A. *Nature* **2007**, *446*, 1023–1029.
(22) Hayashi, N.; Kawasaki, N.; Nakajima, Y.; Toyoda, M.; Katagiri, Y.; Itoh, S.; Harazono, A.; Umezawa, A.; Yamaguchi, T. *J. Chromatogr., A* **2007**, *1160*, 263–269.
(23) Nakamura, K.; Ariga, T.; Yahagi, T.; Miyatake, T.; Suzuki, A.; Yamakawa, T. *J. Biochem.* **1983**, *94*, 1359–1365.
(24) Varki, A. *Glycobiology* **1992**, *2*, 25–40.
(25) Marquina, G.; Waki, H.; Fernandez, L. E.; Kon, K.; Carr, A.; Valiente, O.; Perez, R.; Ando, S. *Cancer Res.* **1996**, *56*, 5165–5171.
(26) Tangvoranuntakul, P.; Gagneux, P.; Diaz, S.; Bardor, M.; Varki, N.; Varki, A.; Muchmore, E. *Proc. Natl. Acad. Sci. U.S.A.* **2003**, *100*, 12045–12050.
(27) Padler-Karavani, V.; Yu, H.; Cao, H.; Chokhawala, H.; Karp, F.; Varki, N.; Chen, X.; Varki, A. *Glycobiology* **2008**, *18*, 818–830.
(28) Ghaderi, D.; Taylor, R. E.; Padler-Karavani, V.; Diaz, S.; Varki, A. *Nat. Biotechnol.* **2010**, *28*, 863–867.
(29) Anumula, K. R.; Dhume, S. T. *Glycobiology* **1998**, *8*, 685–694.
(30) Nakano, M.; Kakehi, K.; Tsai, M.-H.; Lee, Y. C. *Glycobiology* **2004**, *14*, 431–441.
(31) Kamoda, S.; Nakano, M.; Ishikawa, R.; Suzuki, S.; Kakehi, K. *J. Proteome Res.* **2005**, *4*, 146–152.
(32) Naka, R.; Kamoda, S.; Ishizuka, A.; Kinoshita, M.; Kakehi, K. *J. Proteome Res.* **2006**, *5*, 88–97.
(33) Chen, F. T.; Evangelista, R. A. *Electrophoresis* **1998**, *19*, 2639–2644.
(34) Ma, S.; Nashabeh, W. *Anal. Chem.* **1999**, *71*, 5185–5192.
(35) Kakehi, K.; Funakubo, T.; Suzuki, S.; Oda, Y.; Kitada, Y. *J. Chromatogr., A* **1999**, *863*, 205–218.
(36) Raju, T. S. *Anal. Biochem.* **2000**, *283*, 125–132.
(37) Nakajima, K.; Oda, Y.; Kinoshita, M.; Kakehi, K. *J. Proteome Res.* **2003**, *2*, 81–88.
(38) Ma, S.; Lau, W.; Keck, R. G.; Briggs, J. B.; Jones, A. J. S.; Moorhouse, K.; Nashabeh, W. *Methods Mol. Biol.* **2005**, *308*, 397–409.
(39) Ruhaak, L. R.; Zauner, G.; Huhn, C.; Bruggink, C.; Deelder, A. M.; Wuhrer, M. *Anal. Bioanal. Chem.* **2010**, *397*, 3457–3481.
(40) Huhn, C.; Selman, M. H. J.; Ruhaak, L. R.; Deelder, A. M.; Wuhrer, M. *Proteomics* **2009**, *9*, 882–913.
(41) Pabst, M.; Kolarich, D.; Pöltl, G.; Dalik, T.; Lubec, G.; Hofinger, A.; Altmann, F. *Anal. Biochem.* **2009**, *384*, 263–273.
(42) Vultaggio, A.; Matucci, A.; Nencini, F.; Pratesi, S.; Parronchi, P.; Rossi, O.; Romagnani, S.; Maggi, E. *Allergy* **2010**, *65*, 657–661.
(43) Read, E. K.; Park, J. T.; Brorson, K. A. *Biotechnol. Appl. Biochem.* **2011**, *58*, 213–219.
(44) Bardor, M.; Nguyen, D. H.; Diaz, S.; Varki, A. *J. Biol. Chem.* **2005**, *280*, 4228–4237.
(45) Domon, B.; Costello, C. E. *Biochemistry* **1988**, *27*, 1534–1543.

J Nat Med (2012) 66:516–524
DOI 10.1007/s11418-011-0619-6

ORIGINAL PAPER

Anti-hyperlipidemic constituents from the bark of *Shorea roxburghii*

Toshio Morikawa · Saowanee Chaipech · Hisashi Matsuda · Makoto Hamao · Yohei Umeda · Hiroki Sato · Haruka Tamura · Kiyofumi Ninomiya · Masayuki Yoshikawa · Yutana Pongpiriyadacha · Takao Hayakawa · Osamu Muraoka

Received: 7 November 2011 / Accepted: 13 December 2011 / Published online: 20 January 2012

Abstract The methanol extract from the bark of *Shorea roxburghii* (Dipterocarpaceae, "Phayom" in Thai) was found to suppress plasma triglyceride elevation in olive oil-treated mice, and also to inhibit pancreatic lipase activity (IC_{50} = 31.6 μg/ml). From the extract, two new 3-acetyl-4-phenyl-3,4-dihydroisocoumarins, phayomphenols A_1 (**1**) and A_2 (**2**) were isolated, together with 22 known compounds. The structures of **1** and **2** were elucidated on the basis of chemical and spectroscopic evidence, including X-ray crystallographic analysis. Among the isolates, several oligostilbenoids, including (−)-hopeaphenol (**3**) and (+)-isohopeaphenol (**4**), showed inhibitory effects on plasma triglyceride elevation at a dose of 200 mg/kg p.o. and pancreatic lipase inhibitory activity (IC_{50} = 32.9 and 26.5 μM, respectively).

Keywords *Shorea roxburghii* · Dipterocarpaceae · Oligostilbenoid · Anti-hyperlipidemic activity · Pancreatic lipase inhibitor · Phayomphenol

T. Morikawa · S. Chaipech · K. Ninomiya · M. Yoshikawa · T. Hayakawa · O. Muraoka (✉)
Pharmaceutical Research and Technology Institute, Kinki University, 3-4-1 Kowakae, Higashi-Osaka, Osaka 577-8502, Japan
e-mail: muraoka@phar.kindai.ac.jp

H. Matsuda · M. Hamao · Y. Umeda · H. Sato · H. Tamura · M. Yoshikawa
Kyoto Pharmaceutical University, Misasagi, Yamashina-ku, Kyoto 607-8412, Japan

Y. Pongpiriyadacha
Faculty of Science and Technology, Rajamangala University of Technology Srivijaya, Thungsong, Nakhonsithammarat 80110, Thailand

Introduction

A Dipterocarpaceae plant *Shorea roxburghii* G.Don is widely distributed in Thailand and the neighboring countries, Cambodia, India, Laos, Malaysia, Myanmar, and Vietnam. The plant is locally called "Phayom", and its bark has been used for an astringent and preservative for traditional beverages in Thailand. In addition, the bark has also been used for treatments of dysentery, diarrhea, and cholera in Indian folk medicine. A previous chemical study of *S. roxburghii* revealed the presence of several stilbenoids, such as resveratrol and its oligomers [1]. During the course of our characterization studies of Thai medicinal foods [2–6], the methanolic extract from the bark of *S. roxburghii* was found to inhibit plasma triglyceride (TG) elevation in olive oil-treated mice, and also to inhibit pancreatic lipase activity. From the extract, two new 3-acetyl-4-phenyl-3,4-dihydroisocoumarins, named phayomphenols A_1 (**1**) and A_2 (**2**), were isolated, together with 22 known compounds. This paper deals with the structure elucidation of **1** and **2**, as well as the anti-hyperlipidemic activities of these constituents from the bark of *S. roxburghii*.

Results and discussion

The methanol extract (15.56%, IC_{50} for pancreatic lipase = 31.6 μg/ml) from the bark of *S. roxburghii*, collected in Phatthalung Province, Thailand, was subjected to Diaion HP-20 column chromatography (H_2O → MeOH) to give H_2O- and MeOH-eluted fractions (3.17%, >800 μg/ml and 10.61%, 24.3 μg/ml, respectively). As shown in Table 1, the methanolic extract and the MeOH-eluted fraction significantly suppressed plasma TG elevation in mice 2 h after administration of olive oil at a dose of 500 mg/kg p.o.

Table 1 Inhibitory effects of the MeOH extract and its MeOH- and H_2O-eluted fractions from the bark of *S. roxburghii* on plasma triglyceride elevation in olive oil-treated mice

Treatment	Dose (mg/kg p.o.)	*N*	Plasma triglyceride (mg/dL)[a]		
			2.0 h	4.0 h	6.0 h
Normal	–	8	166.7 ± 12.3**	151.2 ± 11.7**	158.1 ± 12.8**
Control	–	12	471.4 ± 36.7	513.8 ± 48.7	359.7 ± 36.2
MeOH extract	125	8	594.6 ± 62.5	526.6 ± 43.4	301.0 ± 31.8
	250	8	494.7 ± 33.7	570.7 ± 86.8	401.5 ± 50.6
	500	8	191.2 ± 23.7**	301.8 ± 52.0*	310.3 ± 27.0
Normal	–	8	159.2 ± 22.8**	125.2 ± 15.9**	113.7 ± 18.6**
Control	–	13	377.0 ± 24.9	420.4 ± 29.6	325.7 ± 42.7
MeOH-eluted fraction	125	7	446.5 ± 88.0	420.1 ± 62.3	305.4 ± 38.3
	250	8	358.8 ± 41.1	397.5 ± 36.5	298.8 ± 38.3
	500	7	83.5 ± 6.5**	110.0 ± 19.7**	128.5 ± 28.3**
H_2O-eluted fraction	250	8	361.0 ± 61.1	380.3 ± 91.9	233.8 ± 53.1
	500	8	353.8 ± 57.4	426.1 ± 55.6	272.3 ± 44.9

Significantly different from the control group, $*p < 0.05$, $**p < 0.01$

[a] Values represent means ± SEM

In order to identify the compounds responsible for the activity, a bioassay-guided separation was conducted. Thus, the MeOH-eluted fraction was subjected to silica gel and ODS column chromatography, and finally HPLC to give phayomphenols A_1 (**1**, 0.29%, from the dried bark) and A_2 (**2**, 0.11%) together with 20 stilbenoids: (−)-hopeaphenol (**3**, 0.63%) [7, 8], (+)-isohopeaphenol (**4**, 0.53%) [7], hemsleyanol D (**5**, 0.30%) [9], (−)-ampelopsin H (**6**, 0.015%) [9], vaticanols B (**7**, 0.031%) [10], C (**8**, 0.032%) [10], A (**9**, 0.28%) [10, 11], E (**10**, 0.30%) [12], and G (**11**, 0.042%) [13], (+)-α-viniferin (**12**, 0.10%) [14], pauciflorol A (**13**, 0.014%) [11], hopeafuran (**14**, 0.012%) [15], (−)-balanocarpol (**15**, 0.070%) [16], (−)-ampelopsin A (**16**, 0.012%) [17], malibatols A (**17**, 0.0029%) [18] and B (**18**, 0.0007%) [18], (+)-parviflorol (**19**, 0.0029%) [17], *trans*-resveratrol 10-*C*-β-D-glucopyranoside (**20**, 0.90%) [19], *cis*-resveratrol 10-*C*-β-D-glucopyranoside (**21**, 0.0081%) [19], and piceid (**22**, 0.0098%) [20], and quercetin 3-*O*-α-L-rhamnopyranoside (0.0050%) [21] and (6*S*,9*S*)-roseoside (0.0017%) [22] (Fig. 1).

Phayomphenol A_1 (**1**) was obtained as a white powder with a positive optical rotation ($[\alpha]_D^{25}$ +157.9 in MeOH). The IR spectrum of **1** showed absorption bands at 3400, 1717, 1613, 1514, 1474, 1362, 1252, and 1125 cm^{-1} ascribable to hydroxy, carbonyl, and lactone carbonyl functions and an aromatic ring. In the EIMS, a molecular ion peak was observed at *m/z* 314 [M^+], and HREIMS analysis indicated the molecular formula to be $C_{17}H_{14}O_6$. The ^1H NMR spectrum (CD_3OD, Table 2) exhibited signals corresponding to a methyl [δ 1.86 (3H, s, H_3-2′)], two methines [δ 4.61, 5.14 (1H each, both d, $J = 4.0$ Hz, H-4, 3)], a 1,2,4,6-tetrasubstituted benzene ring [δ 6.57, 7.04 (1H each, both d, $J = 2.3$ Hz, H-6, 8)], and *ortho*-coupled A_2B_2-type aromatic protons [δ 6.64, 6.82 (2H each, both d, $J = 8.6$ Hz, H-3″,5″, 2″,6″)]. The 3-acetyl-4-phenyl-3,4-dihydroisocoumarin structure in **1** was constructed on the basis of ^1H–^1H COSY, HMQC, and HMBC correlations. Thus, the ^1H–^1H COSY experiments on **1** indicated partial structures shown in bold lines in Fig. 2. In the HMBC experiment, long-range correlations were observed between the following proton and carbon pairs: H-3 and C-1, 10, 1′, 1″; H-4 and C-5, 9, 10, 1″, 2″,6″; H-6 and C-8, 10; H-8 and C-1, 6, 10; H-2″,6″ and C-4, 4″; H-3″,5″ and C-1″; H_3-2′ and C-3, 1′. The relative stereostructure of C-3 and C-4 in the 3,4-dihydroisocoumarin moiety was deduced by nuclear Overhauser effect spectroscopy (NOESY) experiments on **1**, in which the NOE correlations were observed between the following proton pairs: H-3 and H-4; H-4 and H-2″,6″. Next, methylation of **1** with methyl iodide (CH_3I) in the presence of potassium carbonate (K_2CO_3) in *N*,*N*-dimethylformamide (DMF) yielded corresponding 5-monomethyl (**1a**), 5,7-dimethyl (**1b**), and 5,7,4″-trimethyl (**1c**) derivatives. The positions of the methoxyls in **1a** and **1b** were determined on the basis of their NMR spectroscopic properties, including those of HMBC and NOESY experiments. To confirm the stereostructure of **1**, X-ray crystallographic analysis was conducted on its trimethyl derivative (**1c**) as shown in Fig. 3. Thus, the relative stereostructure at C-3 and C-4 in **1** was confirmed to be *cis*-configuration.

Phayomphenol A_2 (**2**) was also obtained as a white powder with a positive optical rotation ($[\alpha]_D^{25}$ +112.3 in MeOH). The positive-ion FABMS showed a quasimolecular ion peak at *m/z* 337 [M + Na]$^+$, and the molecular formula, $C_{17}H_{14}O_6$, was found to be the same as that of **1** by HRFABMS measurement. The ^1H and ^{13}C NMR spectroscopic properties of **2** (CD_3OD, Table 2) were quite similar to those of **1**. That is, **2** showed signals due to a methyl [δ 2.23 (3H, s, H_3-2′)], two methines [δ 4.80 (1H, br s, H-4), 5.28 (1H, d, $J = 1.5$ Hz, H-3)], a 1,2,4,6-tetrasubstituted benzene ring [δ 6.55, 6.99 (1H each, both d, $J = 2.3$ Hz, H-6, 8)], and *ortho*-coupled A_2B_2-type

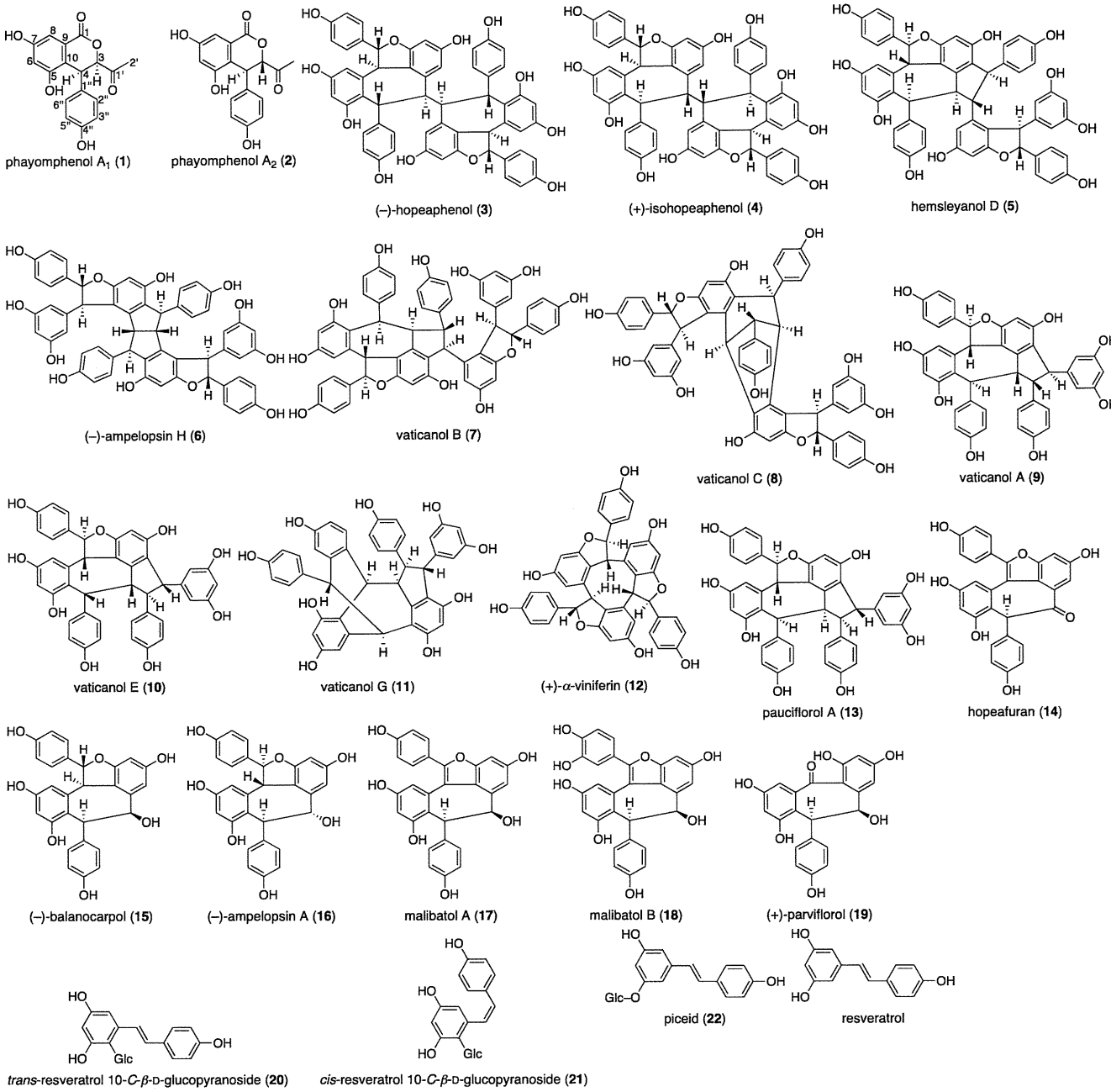

Fig. 1 Constituents from the bark of *S. roxbrghii*

aromatic protons [δ 6.71, 6.96 (2H each, both d, J = 8.6 Hz, H-3″,5″, 2″,6″)]. The planar structure of **2** was characterized to be the same as that of **1** by means of ^{1}H–^{1}H COSY and HMBC experiments as shown in Fig. 2. The NOESY spectrum of **2** showed distinct correlations between the following proton pairs: H-3 and H-2″,6″; H-4 and H-2″,6″ (Fig. 2). Thus, **2** was a diastereoisomer of **1**.

Finally, the absolute stereochemistry of **1** and **2** was elucidated by analysis of their CD spectra, which showed a negative ($\Delta\varepsilon$ −0.45 at 295 nm) and a positive ($\Delta\varepsilon$ +6.96 at 291 nm) Cotton effect, respectively. In accordance with published CD data for 3,4-dihydroisocoumarins, these Cotton effects were assignable to the $n \rightarrow \pi^*$ transition of the lactone carbonyl group of the dihydroisocoumarin chromophore [23, 24]. This indicated that the 3-acetyl group in **2** was in an α-axial orientation, and accordingly the absolute configuration at C-3 of **2** was concluded to be *S* [25–30]. In the same manner, the absolute configuration at C-3 of **1** was determined to be *R*. This result indicated that the 4-hydroxyphenyl moieties at C-4 in **1** and **2** were both in a β-axial orientation, and their absolute configurations were also concluded to be *S*. On the basis of the

Table 2 ^{1}H and ^{13}C NMR spectroscopic data (CD_3OD) of **1** and **2**, and **1a–1c**

Position	**1**		**2**		**1a**		**1b**		**1c**	
	δ_H	δ_C	δ_H	δ_C	δ_H	δ_C	δ_H	δ_C	δ_H	δ_C
1		166.9		166.7		166.6		166.4		166.3
3	5.14 (1H, d, 4.0)	86.7	5.28 (1H, d, 1.5)	89.1	5.14 (1H, d, 3.7)	86.6	5.16 (1H, d, 4.0)	86.5	5.19 (1H, d, 4.0)	86.4
4	4.61 (1H, d, 4.0)	40.2	4.80 (1H, br s)	38.5	4.59 (1H, d, 3.7)	40.1	4.63 (1H, d, 4.0)	40.2	4.67 (1H, d, 4.0)	40.2
5		156.4		156.7		158.4		158.3		158.3
6	6.57 (1H, d, 2.3)	109.7	6.55 (1H, d, 2.3)	109.2	6.70 (1H, d, 2.3)	106.2	6.80 (1H, d, 2.6)	106.0	6.82 (1H, d, 2.3)	106.0
7		159.1		159.3		159.7		161.9		162.0
8	7.04 (1H, d, 2.3)	107.5	6.99 (1H, d, 2.3)	107.5	7.11 (1H, d, 2.3)	107.7	7.23 (1H, d, 2.6)	104.7	7.25 (1H, d, 2.3)	104.7
9		126.9		127.8		126.9		126.9		126.9
10		121.6		117.5		122.9		124.7		124.6
1′		207.6		205.4		207.5		207.6		207.1
2′	1.86 (3H, s)	27.6	2.23 (3H, s)	26.0	1.86 (3H, s)	27.6	1.87 (3H, s)	27.6	1.87 (3H, s)	27.6
1″		128.3		132.4		128.1		127.8		129.2
2″,6″	6.82 (2H, d, 8.6)	131.2	6.96 (2H, d, 8.6)	129.8	6.79 (2H, d, 8.6)	131.1	6.80 (2H, d, 8.9)	131.2	6.91 (2H, d, 8.9)	131.2
3″,5″	6.64 (2H, d, 8.6)	116.1	6.71 (2H, d, 8.6)	116.3	6.63 (2H, d, 8.6)	116.2	6.63 (2H, d, 8.9)	116.2	6.78 (2H, d, 8.9)	114.9
4″		157.9		157.6		158.0		158.1		160.6
5-OCH_3					3.72 (3H, s)	56.4	3.74 (3H, s)	56.5	3.75 (3H, s)	56.5
7-OCH_3							3.86 (3H, s)	56.2	3.87 (3H, s)	56.2
4″-OCH_3									3.72 (3H, s)	55.6

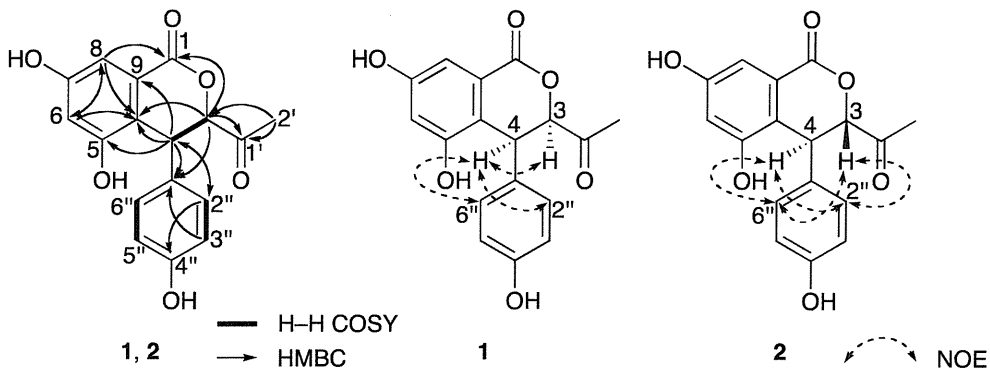

Fig. 2 ^{1}H–^{1}H COSY, HMBC, and NOESY correlations of **1** and **2**

foregoing evidence, the absolute stereochemistries of **1** and **2** were elucidated as (3*R*,4*S*)- and (3*S*,4*S*)-3-acetyl-5,7-dihydroxy-4-(4-hydroxyphenyl)-3,4-dihydroisocoumarin, respectively.

The effects of the principal constituents (**1–5**, **12**, **15** and **20**) from *S. roxburghii* on plasma TG elevation in olive oil-treated mice were examined. As shown in Table 3, orlistat [31] was used as a standard, showing a good activity in this assay model. Among the principal constituents, several oligostilbenoids such as (−)-hopeaphenol (**3**), (+)-isohopeaphenol (**4**), hemsleyanol D (**5**), (+)-α-viniferin (**12**), and (−)-balanocarpol (**15**) significantly suppressed the increase in serum TG levels 2 h after administration of olive oil at a dose of 200 mg/kg p.o.

Pancreatic lipase is well known to have an important role in lipid digestion. Previously, it was reported that the anti-hyperlipidemic effects of oligostilbenoids was ascribable to their pancreatic lipase inhibitory effects [4]. In the course of our characterization studies on bioactive constituents from *S. roxburghii*, inhibitory effects of the constituents on pancreatic lipase activity were examined. As a result, most oligostilbenoid constituents (**3–12**, **14–19**) were found to inhibit pancreatic lipase (IC_{50} range = 9.3–340 μM), although their inhibitory activities were considerably less than that of a lipase inhibitor, orlistat (IC_{50} = 56 nM). Compounds **1**, **2** and resveratrol glycosides (**20** and **21**) did not show such an effect (IC_{50} > 400 μM) (Table 4).

In conclusion, two new 3-acetyl-4-phenyl-3,4-dihydroisocoumarins, phayomphenols A_1 (**1**) and A_2 (**2**), and 22 known compounds were isolated from the methanolic extract of the bark of *S. roxburghii*, which was found to inhibit plasma TG elevation in olive oil-treated mice based on the lipase inhibitory activity (IC_{50} = 31.6 μg/ml) as one

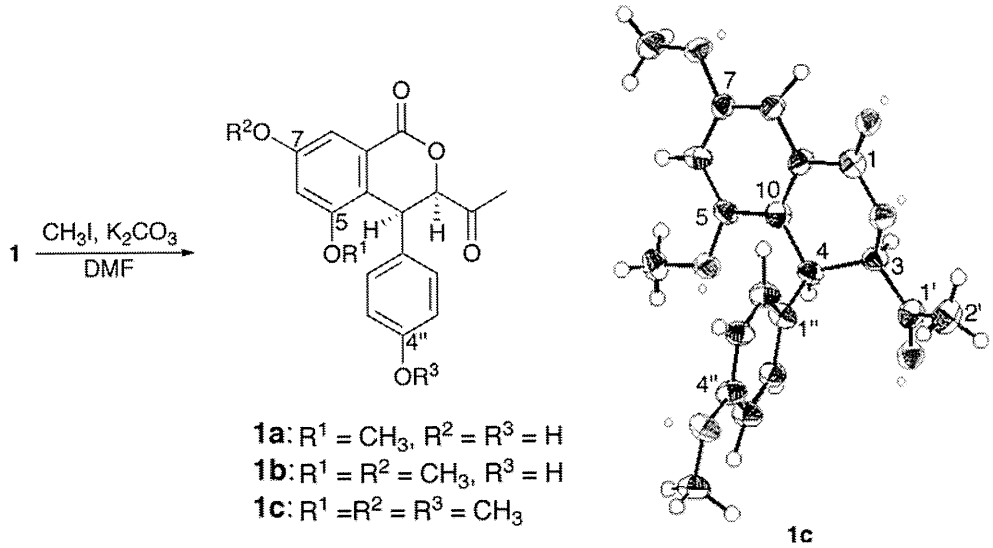

Fig. 3 ORTEP representation of **1c**

of the possible mechanisms of action. Of the isolates, several oligostilbenoids such as (−)-hopeaphenol (**3**), (+)-isohopeaphenol (**4**), hemsleyanol D (**5**), (+)-α-viniferin (**12**), and (−)-balanocarpol (**15**) showed inhibitory effects on plasma triglyceride elevation at a dose of 200 mg/kg p.o. and pancreatic lipase inhibitory activity (IC_{50} = 32.9, 26.5, 23.2, 46.3, and 340 μM, respectively). On the basis of the above-mentioned evidence, the oligostilbenoid constituents from *S. roxburghii* could be potentially useful for prevention of obesity, although further anti-obesity experiments should be performed.

Experimental method

General

The following instruments were used to obtain physical data: specific rotations, Horiba SEPA-300 digital polarimeter (l = 5 cm); CD spectra, JASCO J-720WI spectrometer; UV spectra, Shimadzu UV-1600 spectrometer; IR spectra, Shimadzu FTIR-8100 spectrometer; ^{1}H NMR spectra, JEOL JNM-ECA500 (500 MHz) and JNM-ECS400 (400 MHz) spectrometers; ^{13}C NMR spectra, JEOL JNM-ECA500 (125 MHz) and JNM-ECS400 (100 MHz) spectrometers with tetramethylsilane as an internal standard; EIMS and HREIMS, JEOL JMS-GCMATE mass spectrometer; FAB-MS and HRFABMS, JEOL JMS-SX 102A mass spectrometer; HPLC detector, Shimadzu SPD-10A UV–VIS detector; HPLC column, Cosmosil 5C_{18}-MS-II and πNAP (250 × 4.6 mm i.d.) and (250 × 20 mm i.d.) columns were used for analytical and preparative purposes, respectively.

The following experimental conditions were used for chromatography: normal-phase silica gel column chromatography (CC), silica gel 60 N (Kanto Chemical Co., Ltd., 63–210 mesh, spherical, neutral); reversed-phase silica gel CC, Diaion HP-20 (Nippon Rensui) and Chromatorex ODS DM1020T (Fuji Silysia Chemical, Ltd., 100–200 mesh); TLC, pre-coated TLC plates with silica gel 60F_{254} (Merck, 0.25 mm) (normal-phase) and silica gel RP-18 F_{254S} (Merck, 0.25 mm) (reversed-phase); reversed-phase HPTLC, pre-coated TLC plates with silica gel RP-18 WF_{254S} (Merck, 0.25 mm); detection was carried out by spraying 1% $Ce(SO_4)_2$–10% aqueous H_2SO_4 on the plates, followed by heating.

Plant material

Bark of *Shorea roxburghii* was collected in Phatthalung Province, Thailand in September 2006. The plant material was identified by one of the authors (Y. P.). A voucher specimen (2006.09. Raj-02) of this plant is on file in our laboratory (O. M.).

Extraction and isolation

Dried bark of *S. roxburghii* (3.7 kg) was finely cut and extracted three times with MeOH under reflux conditions for 3 h. Evaporation of the combined extract under reduced pressure provided a MeOH extract (575.7 g, 15.56%). An aliquot (525.7 g) was subjected to Diaion HP-20 CC (3.0 kg, H_2O → MeOH, twice) to give H_2O-eluted (107.0 g, 3.17%) and MeOH-eluted (358.5 g, 10.61%) fractions, respectively. An aliquot (180.0 g) of the MeOH-eluted fraction was subjected to normal-phase silica gel CC [3.0 kg, $CHCl_3$–MeOH–H_2O (10:3:0.4 → 7:3:0.5 → 6:4:1, v/v/v) → MeOH] to give eight fractions [Fr. 1 (2.82 g), Fr. 2 (8.20 g), Fr. 3 (9.20 g), Fr. 4 (66.38 g), Fr. 5 (18.29 g), Fr. 6 (20.11 g), Fr. 7 (25.93 g), and Fr. 8 (31.25 g)]. Fraction 2 (8.20 g) was subjected to reversed-phase silica gel CC

Table 3 Inhibitory effects of the constituents from the bark of *S. roxburghii* on plasma triglyceride elevation in olive oil-treated mice

Treatment	Dose (mg/kg p.o.)	*N*	Plasma triglyceride (mg/dL)[a]		
			2.0 h	4.0 h	6.0 h
Normal	–	6	114.9 ± 18.1**	110.4 ± 12.0**	134.6 ± 7.7**
Control	–	8	546.7 ± 59.4	375.9 ± 66.2	271.5 ± 62.5
Phayomphenol A_1 (**1**)	100	8	580.6 ± 51.2	491.7 ± 72.0	454.2 ± 81.2
	200	8	599.4 ± 65.6	459.5 ± 57.6	352.1 ± 56.6
Phayomphenol A_2 (**2**)	100	8	549.4 ± 70.0	298.1 ± 48.1	282.0 ± 50.5
	200	8	217.5 ± 51.7**	401.6 ± 80.1	412.3 ± 46.8
Resveratrol	100	8	408.4 ± 50.7	388.3 ± 57.0	497.8 ± 55.0
	200	8	332.9 ± 63.0	528.0 ± 100.0	452.8 ± 87.0
Normal	–	10	80.4 ± 10.9**	81.4 ± 11.2**	66.5 ± 9.6**
Control	–	14	518.7 ± 63.1	404.0 ± 72.6	174.4 ± 21.0
(−)-Hopeaphenol (**3**)	100	8	393.4 ± 45.0	338.3 ± 36.6	203.0 ± 28.8
	200	7	269.5 ± 56.8**	139.6 ± 25.7**	127.3 ± 16.2
(+)-Isohopeaphenol (**4**)	100	8	378.7 ± 49.7	296.7 ± 59.2	166.1 ± 35.7
	200	8	237.2 ± 36.2**	176.0 ± 20.4**	148.0 ± 13.7
Hemsleyanol D (**5**)	100	4	580.0 ± 186.5	537.9 ± 111.7	275.9 ± 67.1
	200	4	274.6 ± 26.4**	172.7 ± 25.1*	118.5 ± 37.0
(+)-α-Viniferin (**12**)	100	8	368.6 ± 37.5	249.9 ± 31.5	170.8 ± 27.0
	200	8	266.9 ± 40.3**	156.5 ± 19.9**	97.7 ± 10.7
(−)-Balanocarpol (**15**)	100	8	512.9 ± 61.0	372.7 ± 37.1	219.7 ± 33.9
	200	8	240.5 ± 37.7**	244.7 ± 49.6	146.9 ± 27.7
Normal	–	8	158.9 ± 20.9**	195.3 ± 15.0**	143.9 ± 20.1**
Control	–	8	483.5 ± 36.1	500.5 ± 53.4	297.4 ± 25.2
trans-Resveratrol 10-*C*-β-D-Glucopyranoside (**20**)	100	8	475.7 ± 28.8	424.4 ± 43.2	261.8 ± 33.9
	200		452.9 ± 49.8	383.6 ± 38.0	259.3 ± 26.3
Normal	–	7	91.9 ± 9.4**	97.3 ± 7.4**	90.6 ± 9.4**
Control	–	9	440.3 ± 60.2	393.2 ± 60.1	263.3 ± 45.0
Orlistat	5	7	371.3 ± 41.5	297.0 ± 67.4	171.9 ± 24.9
	10	7	203.8 ± 52.1**	160.4 ± 47.7**	129.1 ± 16.6**
	20	7	198.6 ± 24.1**	131.0 ± 16.8**	114.5 ± 7.6**

Significantly different from the control group, $*p < 0.05$, $**p < 0.01$

[a] Values represent the means ± SEM

[250 g, MeOH–H_2O (20:80 → 40:60 → 50:50, v/v) → MeOH] to afford seven fractions [Fr. 2-1 (4.8 mg), Fr. 2-2 (41.1 mg), Fr. 2-3 (55.3 mg), Fr. 2-4 (774.3 mg), Fr. 2-5 (1256.3 mg), Fr. 2-6 (5540.5 mg), and Fr. 2-7 (1081.9 mg)]. Fraction 2-4 (500.4 mg) was purified by HPLC [Cosmosil $5C_{18}$-MS-II, MeOH–1% aqueous AcOH (20:80, v/v)] to give phayomphenols A_1 (**1**, 6.4 mg, 0.0006%) and A_2 (**2**, 442.6 mg, 0.040%). Fraction 2-5 (500.7 mg) was purified by HPLC [Cosmosil $5C_{18}$-MS-II, MeOH–1% aqueous AcOH (30:70, v/v)] to give **1** (123.0 mg, 0.018%) and **2** (165.4 mg, 0.025%). Fraction 2-6 (500.1 mg) was purified by HPLC [Cosmosil $5C_{18}$-MS-II, MeOH–1% aqueous AcOH (40:60, v/v)] to give **1** (14.4 mg, 0.0094%), **2** (61.9 mg, 0.040%), and (+)-α-viniferin (**12**, 154.6 mg, 0.10%). Fraction 3 (9.20 g) was subjected to reversed-phase silica gel CC [280 g, MeOH–H_2O (40:60 → 50:50, v/v) → MeOH] to afford seven fractions [Fr. 3-1 (268.7 mg), Fr. 3-2 (1408.4 mg), Fr. 3-3 [= (−)-balanocarpol (**15**, 404.6 mg, 0.024%)], Fr. 3-4 (454.8 mg), Fr. 3-5 (1650.4 mg), Fr. 3-6 (1835.4 mg), and Fr. 3-7 (1263.6 mg)]. Fraction 3-1 (268.7 mg) was further separated by HPLC [Cosmosil $5C_{18}$-MS-II, MeOH–1% aqueous AcOH (25:75, v/v)] to furnish **2** (45.6 mg, 0.0027%). Fraction 3-2 (500.7 mg) was further separated by HPLC [Cosmosil $5C_{18}$-MS-II, MeOH–1% aqueous AcOH (25:75, v/v)] to furnish **1** (5.8 mg, 0.0010%), **2** (17.3 mg, 0.0029%), **15** (277.6 mg, 0.046%), (−)-ampelopsin A (**16**, 70.9 mg, 0.012%), (+)-parviflorol (**19**, 17.5 mg, 0.0029%), and (6*S*,9*S*)-roseoside (10.3 mg, 0.0017%). Fraction 3-4 (454.8 mg) was further separated by HPLC [Cosmosil $5C_{18}$-MS-II, MeOH–1% aqueous AcOH (40:60, v/v)] to furnish

Table 4 IC_{50} Values of the constituents from the bark of *S. roxburghii* for pancreatic lipase

Test samples	IC_{50} (μM)
Phayomphenol A_1 (**1**)	>400
Phayomphenol A_2 (**2**)	>400
(−)-Hopeaphenol (**3**)	32.9
(+)-Isohopeaphenol (**4**)	26.5
Hemsleyanol D (**5**)	23.2
(−)-Ampelopsin H (**6**)	9.3
Vaticanol B (**7**)	25.1
Vaticanol C (**8**)	12.5
Vaticanol A (**9**) [4]	51.7
Vaticanol E (**10**) [4]	85.5
Vaticanol G (**11**) [4]	58.8
(+)-α-Viniferin (**12**)	46.3
Hopeafuran (**14**)	26.6
(−)-Balanocarpol (**15**)	340
(−)-Ampelopsin A (**16**)	140
Malibatol A (**17**)	60.8
Malibatol B (**18**)	43.4
(+)-Parviflorol (**19**)	284
trans-Resveratrol 10-*C*-β-D-glucopyranoside (**20**)	>400
cis-Resveratrol 10-*C*-β-D-glucopyranoside (**21**)	>400
Resveratrol	>400
Orlistat	0.056

malibatols A (**17**, 49.2 mg, 0.0029%) and B (**18**, 11.5 mg, 0.0007%), and quercetin 3-*O*-α-L-rhamnopyranoside (12.5 mg, 0.0007%). Fraction 3-5 (500.0 mg) was purified by HPLC [Cosmosil $5C_{18}$-MS-II, MeOH–1% aqueous AcOH (40:60, v/v)] to give hopeafuran (**14**, 37.1 mg, 0.0072%) and quercetin 3-*O*-α-L-rhamnopyranoside (25.5 mg, 0.0050%). Fraction 3-6 (500.6 mg) was purified by HPLC [Cosmosil $5C_{18}$-MS-II, MeOH–1% aqueous AcOH (40:60, v/v)] to give **14** (23.0 mg, 0.0050%). Fraction 4 (66.38 g) was subjected to reversed-phase silica gel CC [2.0 kg, MeOH–H_2O (30:70 → 40:60, v/v) → MeOH] to afford six fractions [Fr. 4-1 (0.41 g), Fr. 4-2 [= *trans*-resveratrol 10-*C*-β-D-glucopyranoside (**20**, 10.55 g, 0.62%)], Fr. 4-3 (6.90 g), Fr. 4-4 (20.63 g), Fr. 4-5 (20.32 g), and Fr. 4-6 (4.60 g)]. Fraction 4-3 (500.4 mg) was further purified by HPLC [Cosmosil $5C_{18}$-MS-II, MeOH–1% aqueous AcOH (30:70, v/v)] to furnish (−)-hopeaphenol (**3**, 10.5 mg, 0.0085%), (+)-isohopeaphenol (**4**, 11.6 mg, 0.0094%), pauciflorol A (**13**, 17.3 mg, 0.014%), **20** (121.0 mg, 0.098%), *cis*-resveratrol 10-*C*-β-D-glucopyranoside (**21**, 10.0 mg, 0.0081%), and piceid (**22**, 12.1 mg, 0.0098%). Fraction 4-4 (500.4 mg) was separated by HPLC [Cosmosil $5C_{18}$-MS-II, MeOH–1% aqueous AcOH (40:60, v/v)] to give hemsleyanol D (**5**, 73.7 mg, 0.18%), vaticanols C (**8**, 9.0 mg, 0.022%), A (**9**, 95.8 mg, 0.23%), and E (**10**, 33.6 mg, 0.082%), and **20** (34.7 mg, 0.084%). Fraction 4-5 (500.0 mg) was purified by HPLC [Cosmosil $5C_{18}$-MS-II, MeOH–1% aqueous AcOH (40:60, v/v)] to give **5** (48.0 mg, 0.11%), **9** (19.4 mg, 0.046%), and **10** (88.5 mg, 0.21%). Fraction 5 (18.29 g) was subjected to reversed-phase silica gel CC [540 g, MeOH–H_2O (20:80 → 30:70 → 50:50, v/v) → MeOH] to afford 10 fractions [Fr. 5-1 (909.1 mg), Fr. 5-2 (139.1 mg), Fr. 5-3 (415.3 mg), Fr. 5-4 [= **20** (1592.7 mg, 0.094%), Fr. 5-5 [= **3** (2642.6 mg, 0.16%), Fr. 5-6 (1834.2 mg), Fr. 5-7 [= **4** (4013.6 mg, 0.24%), Fr. 5-8 (5490.9 mg), Fr. 5-9 (749.3 mg), and Fr. 5-10 (489.8 mg)]. Fraction 5-6 (507.3 mg) was further purified by HPLC [Cosmosil $5C_{18}$-MS-II, MeOH–1% aqueous AcOH (30:70, v/v)] to afford **4** (102.1 mg, 0.022%). Fraction 5-8 (500.1 mg) was purified by HPLC [Cosmosil $5C_{18}$-MS-II, MeOH–1% aqueous AcOH (40:60, v/v) and Cosmosil πNAP, MeOH–1% aqueous AcOH (40:60, v/v)] to give **3** (9.6 mg, 0.0062%), **4** (16.8 mg, 0.011%), (−)-ampelopsin H (**6**, 23.7 mg, 0.015%), vaticanol B (**7**, 47.5 mg, 0.031%), and **8** (16.2 mg, 0.011%). Fraction 5-9 (475.5 mg) was purified by HPLC [Cosmosil $5C_{18}$-MS-II, MeOH–1% aqueous AcOH (40:60, v/v)] to give **5** (84.0 mg, 0.0078%) and **10** (31.0 mg, 0.0029%). Fraction 6 (450.0 mg) was separated by HPLC [Cosmosil $5C_{18}$-MS-II, MeOH–1% aqueous AcOH (30:70, v/v)] to give **3** (175.4 mg, 0.46%), **5** (95.9 mg, 0.25%), and vaticanol G (**11**, 15.9 mg, 0.042%).

*Phayomphenol A_1 (**1**)*

White powder, $[\alpha]_D^{25}$ +157.9 (*c* 0.15, MeOH). CD [MeOH, nm (Δε)]: 213 (+28.54), 229 (−25.99), 269 (+7.88), 295 (−0.45), 323 (+1.81). UV λ_{max} (MeOH) nm (log ε): 263 (3.73), 328 (3.50). IR ν_{max} (KBr) cm^{-1}: 3400, 1717, 1613, 1514, 1474, 1362, 1252, 1125. ^1H and ^{13}C NMR data, see Table 2; EIMS *m/z* (%): 314 (M^+, 48), 243 (100). HREIMS *m/z*: 314.0785 [M^+] (calcd for $C_{17}H_{14}O_6$, 314.0790).

*Phayomphenol A_2 (**2**)*

White powder, $[\alpha]_D^{25}$ +112.3 (*c* 0.16, MeOH). CD [MeOH, nm (Δε)]: 214 (+23.09), 229 (−30.91), 271 (+6.42), 291 (+6.96). UV λ_{max} (MeOH) nm (log ε): 261 (3.80), 326 (3.55). IR ν_{max} (KBr) cm^{-1}: 3482, 1728, 1692, 1613, 1514, 1468, 1352, 1196, 1125. ^1H and ^{13}C NMR data, see Table 2; Positive-ion FABMS *m/z* 337 $[M + Na]^+$. HRFABMS *m/z*: 337.0695 $[M + Na]^+$ (calcd for $C_{17}H_{14}O_6Na$, 337.0688).

*Methylation of **1***

A solution of **1** (20.2 mg) in *N*,*N*-dimethylformamide (DMF, 2.0 ml) was treated with methyl iodide (CH_3I,

80 μl) in the presence of potassium carbonate (K_2CO_3, 44 mg), and the mixture was stirred at room temperature for 20 h. The reaction mixture was poured into ice-cooled water, then extracted with EtOAc. The EtOAc extract was washed with brine, then dried over $MgSO_4$ powder and filtered. Evaporation of the filtrate under reduced pressure yielded a residue, which was purified by HPLC [Cosmosil $5C_{18}$-MS-II, MeOH–1% aqueous acetic acid (50:50, v/v)] to furnish **1a** (2.5 mg, 11.8%), **1b** (8.7 mg, 39.5%), and **1c** (9.6 mg, 41.9%) (Fig. 3).

*Compound **1a***

White powder, $[\alpha]_D^{24}$ +119.0 (*c* 0.13, MeOH). UV λ_{max} (MeOH) nm (log ε): 258 (3.61), 326 (3.45). IR ν_{max} (KBr) cm^{-1}: 3400, 1734, 1717, 1509, 1362, 1132. ^1H and ^{13}C NMR data, see Table 2. Positive-ion FABMS *m/z* 351 $[M + Na]^+$. HRFABMS *m/z*: 351.0840 $[M + Na]^+$ (calcd for $C_{18}H_{16}O_6Na$, 351.0845).

*Compound **1b***

White powder, $[\alpha]_D^{24}$ +234.6 (*c* 0.11, MeOH). UV λ_{max} (MeOH) nm (log ε): 259 (3.81), 322 (3.67). IR ν_{max} (KBr) cm^{-1}: 3400, 1732, 1717, 1609, 1541, 1458, 1364, 1202, 1134, 1046. ^1H and ^{13}C NMR data, see Table 2. Positive-ion FABMS *m/z* 365 $[M + Na]^+$. HRFABMS *m/z*: 365.0997 $[M + Na]^+$ (calcd for $C_{19}H_{18}O_6Na$, 365.1001).

*Compound **1c***

Colorless needles, mp 128.8–129.8°C (from MeOH). $[\alpha]_D^{24}$ +141.9 (*c* 0.09, MeOH). UV λ_{max} (MeOH) nm (log ε): 258 (3.68), 321 (3.53). IR ν_{max} (KBr) cm^{-1}: 3400, 1734, 1719, 1609, 1509, 1458, 1362, 1252, 1132, 1044. ^1H and ^{13}C NMR data, see Table 2. Positive-ion FABMS *m/z* 379 $[M + Na]^+$. HRFABMS *m/z*: 379.1152 $[M + Na]^+$ (calcd for $C_{20}H_{20}O_6Na$, 379.1158).

*Crystal data for **1c***

Colorless needles, mp 128.8–129.8°C (from MeOH). $C_{20}H_{20}O_6$, $M = 356.37$. Crystal dimensions: 0.37 × 0.08 × 0.05 mm, crystal system: tetragonal, lattice type: primitive, lattice parameters: $a = 9.1153(2)$, $c = 20.7787(4)$ Å, $V = 1726.48(6)$ $Å^3$, space group: $P4_1$ (#76); $Z = 4$, $D_{calc} = 1.371$ g/cm^3, $F_{000} = 752.00$, μ(CuKα) = 8.445 cm^{-1}, structure solution: Direct Methods (SHELEXS-97), residuals: $R1 = 0.0645$, $R = 0.1157$, $wR2 = 0.1738$, goodness of fit indicator: 1.054. All measurements were made on a Rigaku RAXIS-RAPID diffractometer with graphite monochromated CuKα ($\lambda = 1.54178$ Å) radiation and a rotating anode generator.

Animals

Male ddY mice weighing about 25–30 g were purchased from Kiwa Laboratory Animal Co., Ltd., Wakayama, Japan. The animals were housed at a constant temperature of 23 ± 2°C, and were then fed a standard laboratory chow (MF, Oriental Yeast Co., Ltd., Tokyo, Japan). The animals were fasted for 20–24 h prior to the beginning of the experiment, but were allowed free access to tap water. All of the experiments were performed with conscious mice unless otherwise noted. The experimental protocol was approved by the Experimental Animal Research Committee at Kyoto Pharmaceutical University.

Inhibitory effect on plasma triglyceride (TG) elevation in olive oil-treated mice

Each test sample was administered orally to fasted mice, and olive oil (5 ml/kg) was administered p.o. 30 min later. Blood samples (c. 0.3 ml) were collected in polyethylene tubes (1.5 ml) containing heparin (5 units/tube) from the infraorbital venosus plexus, 2, 4, and 6 h after olive oil treatment. Plasma TG was determined by an enzymatic method using a Triglyceride E-test Wako (Wako Pure Chemical Industries Ltd., Osaka, Japan) [3, 32].

Effect on pancreatic lipase activity

A suspension of triolein (80 mg), phosphatidylcholine (10 mg), and sodium taurocholate (5 mg) in 0.1 M Tris–HCl buffer (pH 7.0, 9 ml) containing 0.1 M NaCl was homogenized for 10 min. This substrate suspension (0.1 ml) in a test tube was pre-incubated with 5 μl of a test sample in DMSO and 95 μl of the Tris–HCl buffer for 3 min at 37°C. An aliquot of porcine pancreatic lipase (250 μg/ml, type II, Sigma Chemical Co.) (50 μl) or the Tris–HCl buffer (50 μl) for a blank test was then added to start the reaction. After 30 min of incubation, the test tube was immediately immersed in boiling water for 2 min to stop the reaction, then cooled with water. Free fatty acid concentration was determined by a commercial kit (NEFA C-test Wako, Wako Pure Chemical Industries, Ltd.). Orlistat was used as a reference compound. IC_{50} was determined graphically ($N = 2$–4) [2, 33].

Statistics

Values were expressed as means ± SEM. For statistical analysis, one-way analysis of variance followed by Dunnett's test was used.

Acknowledgments This work was supported by High-tech Research Center Project for Private Universities: matching fund

subsidy from MEXT (The Ministry of Education, Culture, Sports, Science and Technology), 2007-2011 and also supported by a Grant-in Aid for Scientific Research by JSPS (Japan Society for the Promotion of Science).

References

1. Patcharamun W, Sichaem J, Siripong P, Khumkratok S, Jongaramruang J, Tip-pyang S (2011) A new dimeric resveratrol from the roots of *Shorea roxburghii*. Fitoterapia 82:489–492
2. Morikawa T, Xie Y, Asao Y, Okamoto M, Yamashita C, Muraoka O, Matsuda H, Pongpiriyadacha Y, Yuan D, Yoshikawa M (2009) Oleanane-type triterpene oligoglycosides with pancreatic lipase inhibitory activity from the pericarps of *Sapindus rarak*. Phytochemistry 70:1166–1172
3. Asao Y, Morikawa T, Xie Y, Okamoto M, Hamao M, Matsuda H, Muraoka O, Yuan D, Yoshikawa M (2009) Structures of acetylated oleanane-type triterpene saponins, rarasaponins IV, V, and VI, and anti-hyperlipidemic constituents from the pericarps of *Sapindus rarak*. Chem Pharm Bull 57:198–203
4. Matsuda H, Asao Y, Nakamura S, Hamao M, Sugimoto S, Hongo M, Pongpiriyadacha Y, Yoshikawa M (2009) Antidiabetogenic constituents from the Thai traditional medicine *Cotylelobium melanoxylon*. Chem Pharm Bull 57:487–494
5. Matsuda H, Ninomiya K, Morikawa T, Yasuda D, Yamaguchi I, Yoshikawa M (2009) Hepatoprotective amide constituents from the fruit of *Piper chaba*: structural requirements, mode of action, and new amides. Bioorg Med Chem 17:7313–7323
6. Muraoka O, Morikawa T, Miyake S, Akaki J, Ninomiya K, Pongpiriyadacha Y, Yoshikawa M (2011) Quantitative analysis of neosalacinol and neokotalanol, another two potent α-glucosidase inhibitors from *Salacia* species, by LC–MS with ion pair chromatography. J Nat Med 65:142–148
7. Ito T, Abe N, Oyama M, Iinuma M (2008) Oligostilbenoids from Dipterocarpaceaeous plants: a new resveratrol tetramer from *Vateria indica* and the revised structure of isohopeaphenol. Helv Chim Acta 91:1989–1998
8. Ito T, Abe N, Masuda Y, Nasu M, Oyama M, Sawa R, Takahashi Y, Iinuma M (2009) Two novel resveratrol derivatives from the leaves of *Vateria indica*. Helv Chim Acta 92:195–208
9. Tanaka T, Ito T, Nakaya K, Iinuma M, Takahashi Y, Naganawa H, Riswan S (2001) Six new heterocyclic stilbene oligomers from stem bark of *Shorea hemsleyana*. Heterocycles 55:729–740
10. Tanaka T, Ito T, Nakaya K, Iinuma M, Riswan S (2000) Oligostilbenoids in stem bark of *Vatica rassak*. Phytochemistry 54:63–69
11. Ito T, Tanaka T, Iinuma M, Iliya I, Nakaya K, Ali Z, Takahashi Y, Sawa R, Shirataki Y, Murata J, Darnaedi D (2003) New resveratrol oligomers in the stem bark of *Vatica pauciflora*. Tetrahedron 59:5347–5363
12. Ito T, Tanaka T, Ido Y, Nakaya K, Iinuma M, Takahashi Y, Naganawa H, Riswan S (2001) Five new oligostilbenes with one or two dihydrofurans from the stem bark of *Vatica rassak*. Heterocycles 55:557–567
13. Ito T, Tanaka T, Nakaya K, Iinuma M, Takahashi Y, Naganawa H, Ohyama M, Nakanishi Y, Bastow KF, Lee K-H (2001) A novel bridged stilbenoid trimer and four highly condensed stilbenoid oligomers in *Vatica rassak*. Tetrahedron 57:7309–7321
14. Kitanaka S, Ikezawa T, Yasukawa K, Yamanouchi S, Takido M, Sung HK, Kim IH (1990) (+)-α-Viniferin, an anti-inflammatory compound from *Caragana chamlagu* root. Chem Pharm Bull 38:432–435
15. Tanaka T, Ito T, Ido Y, Nakaya K, Iinuma M, Chelladurai V (2001) Hopeafuran and a *C*-glucosyl resveratrol isolated from stem wood of *Hopea utilis*. Chem Pharm Bull 49:785–787
16. Diyasena MNC, Sotheeswaran S, Surendrakumar S, Balasubramanian S, Bokel M, Kraus W (1985) Balanocarpol a new polyphenol from *Balanocarpus zeylanicus* (Trimen) and *Hopea jucunda* (Thw.) (Dipterocarpaceae). J Chem Soc Perkin Trans I:1807–1809
17. Tanaka T, Ito T, Ido Y, Son T-K, Nakaya K, Iinuma M, Ohyama M, Chelladurai V (2000) Stilbenoids in the stem bark of *Hopea parviflora*. Phytochemistry 53:1015–1019
18. Dai J-R, Hallock YF, Cardellina JH II, Boyd MR (1998) HIV-inhibitory and cytotoxic oligostilbenes from the leaves of *Hopea malibato*. J Nat Prod 61:351–353
19. Baderschneider B, Winterhalter P (2000) Isolation and characterization of novel stilbene derivatives from Riesling wine. J Agric Food Chem 48:2681–2686
20. Jayatilake GS, Jayasuriya H, Lee E-S, Koonchanok NM, Geahlen RL, Ashendel CL, McLaughlin JL, Chang C-J (1993) Kinase inhibitors from *Polygonum cuspidatum*. J Nat Prod 56:1805–1810
21. Markham KR, Ternai B, Stanley R, Geiger H, Mabry TJ (1978) Carbon-13 NMR studies of flavonoids-III naturally occurring flavonoid glycosides and their acylated derivatives. Tetrahedron 34:1389–1397
22. Yamano Y, Ito M (2005) Synthesis of optically active vomifoliol and roseoside stereoisomers. Chem Pharm Bull 53:541–546
23. Magid AA, Voutquenne-Nazabadioko L, Moroy G, Moretti C, Lavaud C (2007) Dihydroisocoumarin glucosides from stem bark of *Caryocar glabrum*. Phytochemistry 68:2439–2443
24. Duan W-J, Jin X, Chen L-X, Zhang X, Yao X-S, Qiu F (2009) Four new compounds from *Paeonia albiflora*. J Asian Nat Prod Res 11:297–303
25. Hashimoto T, Tori M, Asakawa Y (1987) Three dihydroisocoumarin glucosides from *Hydrangea macrophylla* subsp. *serrata*. Phytochemistry 26:3323–3330
26. Speranza G, Manitto P, Cassara P, Monti D (1993) Feralolide, a dihydroisocoumarin from *Cape aloe*. Phytochemistry 33:175–178
27. Krohn K, Bahramsari R, Flörke U, Ludewig K, Kliche-Spory C, Michel A, Aust H-J, Draeger S, Schulz B, Antus S (1997) Dihydroisocoumarins from fungi: isolation, structure elucidation, circular dichroism and biological activity. Phytochemistry 45:313–320
28. Ito C, Mishina Y, Litaudon M, Cosson J-P, Furukawa H (2000) Xanthone and dihydroisocoumarin from *Montrouziera sphaeroidea*. Phytochemistry 53:1043–1046
29. Kurosaki Y, Fukuda T, Iwao M (2005) Asymmetric synthesis of 3-substituted 3,4-dihydroisocoumarins via stereoselective addition of laterally lithiated chiral 2-(*o*-tolyl)oxazolines to aldehydes followed by diastereomer-selective lactonization. Tetrahedron 61:3289–3303
30. Zidorn C, Lohwasser U, Pschorr S, Salvenmoser D, Ongania K-H, Ellmerer EP, Börner A, Stuppner H (2005) Bibenzyls and dihydroisocoumarins from white salsify (*Tragopogon porrifolius* subsp. *porrifolius*). Phytochemistry 66:1691–1697
31. McNeely W, Benfield P (1998) Orlistat. Drugs 56:241–249
32. Morikawa T, Li X, Nishida E, Ito Y, Matsuda H, Nakamura S, Muraoka O, Yoshikawa M (2008) Perennisosides I–VII, acylated triterpene saponins with antihyperlipidemic activities from the flowers of *Bellis perennis*. J Nat Prod 71:828–835
33. Morikawa T, Li X, Nishida E, Nakamura S, Ninomiya K, Matsuda H, Oda Y, Muraoka O, Yoshikawa M (2010) Medicinal flowers. Part 29. acylated oleanane-type triterpene bisdesmosides: perennisaponins G, H, I, J, K, L, and M with pancreatic lipase inhibitory activity from the flowers of *Bellis perennis*. Helv Chim Acta 93:573–586